NASA TECHNICAL NOTE

NASA TN D-5943

MEASURED AND PREDICTED LONGITUDINAL VIBRATIONS OF A LIQUID PROPELLANT TWO-STAGE LAUNCH VEHICLE

by Robert R. Clary and Lloyd J. Turner, Jr.

Langley Research Center
Hampton, Va. 23365

NATIONAL AERONAUTICS AND SPACE ADMINISTRATION • WASHINGTON, D. C. • AUGUST 1970

1. Report No.	2. Government Accession No.	3. Recipient's Catalog No.
NASA TN D-5943		

4. Title and Subtitle
MEASURED AND PREDICTED LONGITUDINAL VIBRATIONS OF A LIQUID PROPELLANT TWO-STAGE LAUNCH VEHICLE

5. Report Date: August 1970

6. Performing Organization Code:

7. Author(s)
Robert R. Clary and Lloyd J. Turner, Jr.

8. Performing Organization Report No.: L-6646

9. Performing Organization Name and Address
NASA Langley Research Center
Hampton, Va. 23365

10. Work Unit No.: 124-08-13-04

11. Contract or Grant No.:

12. Sponsoring Agency Name and Address
National Aeronautics and Space Administration
Washington, D.C. 20546

13. Type of Report and Period Covered: Technical Note

14. Sponsoring Agency Code:

15. Supplementary Notes

16. Abstract

An experimental and analytical program was conducted to investigate the longitudinal vibration properties of a two-stage full-scale launch vehicle loaded with various amounts of simulated propellants. A two-dimensional finite-element mathematical model formulated from vehicle physical parameters and experimental results was the basis for free- and forced-vibration analyses. Good agreement was obtained between the measured and predicted responses. Vector-response plots enhanced the interpretation of experimental and forced-vibration analytical results. Proper identification and correlation of the modes required a knowledge of the accelerations along the length of the vehicle, accelerations of specific components such as the engines and the turbopump, and pressures at the top and bottom of the propellant tanks.

17. Key Words (Suggested by Author(s))	18. Distribution Statement
Longitudinal vibrations Launch vehicle vibrations Data interpretation techniques Finite element analysis	Unclassified – Unlimited

19. Security Classif. (of this report)	20. Security Classif. (of this page)	21. No. of Pages	22. Price*
Unclassified	Unclassified	60	$3.00

*For sale by the Clearinghouse for Federal Scientific and Technical Information
Springfield, Virginia 22151

MEASURED AND PREDICTED LONGITUDINAL VIBRATIONS OF A LIQUID PROPELLANT TWO-STAGE LAUNCH VEHICLE

By Robert R. Clary and Lloyd J. Turner, Jr.
Langley Research Center

SUMMARY

An experimental and analytical program was conducted to investigate the longitudinal vibration characteristics of a two-stage full-scale launch vehicle which contained simulated propellants adjusted to represent various flight-weight conditions. A two-dimensional finite-element mathematical model was the basis for both free- and forced-vibration analyses. Results of these analyses are compared with each other and with experimental results. Polar plots of acceleration vectors were used to obtain natural frequencies, mode shapes, and modal damping factors from experimental and analytical results.

Concurrent use of phase and magnitude of experimental and analytical response data provided an efficient and accurate means of determining vehicle resonant frequencies and response shapes. Results obtained from vector-response plots of the experimental data agreed well with results determined from the harmonic analysis of peak-response experimental data. Vector-response plots also provided a practical means of acquiring modal damping data.

The forced-vibration analysis was useful in describing the relative importance and prominence of various modes and aided in interpreting and understanding the experimental data. The free- and forced-vibration analyses accurately predicted the resonant frequencies and response shapes of the vehicle for all weight conditions. However, experimental data were necessary to obtain adequate mathematical representations of major components such as the turbopump and the thrust structure.

INTRODUCTION

During the development of any large and complex multistage launch vehicle, significant effort is directed toward understanding its structural dynamic characteristics. Extensive studies of the vehicle must be conducted to verify its structural integrity, to ascertain its dynamic-response properties, and to provide data necessary for evaluation of potential instabilities associated with both the structure and the control systems.

These studies are normally accomplished through use of combined analytical and experimental investigations of the full-size vehicle which is often costly and time consuming. Because information is needed early in the development cycle, an attractive alternate to testing the full-scale vehicle is the use of reduced-scale dynamic models to guide and verify analyses. There exists a degree of uncertainty as to the capability of the analytical and experimental model structural components to represent properly the full-scale parts such as the engines and thrust structure. Accordingly, comparative studies of analyses, full-scale structures, and/or reduced scale models have been carried out. (For example, see refs. 1 to 6.) However, most of these studies have dealt primarily with lateral or bending modes of vibration since, as with aircraft, the designer has been concerned primarily with these modes rather than with the longitudinal modes. Considerable interest in longitudinal response has been generated in recent years by a need for a better understanding of the pogo phenomenon which has caused severe longitudinal oscillations in several multistage launch vehicles. Pogo is an instability caused by coupling of a longitudinal vibration mode with the dynamics of a propellant feed system and engine operation. For the Titan III and Saturn 5 vehicles, longitudinal vibration studies were made by using analyses and reduced-scale model experiments (refs. 5 and 6) but no comparisons were available between analyses and full-scale vehicle tests. Thus, there existed a need for in-depth associated experimental and analytical studies to determine the longitudinal vibration properties of a representative liquid-propellant full-scale multistage launch vehicle. To meet this need, a Thor (model DM-18A) and Agena-B vehicle were obtained.

Longitudinal vibration studies were initially carried out for the isolated Thor and Agena. A free-vibration analysis in which the mathematical models consist of a series of rigid masses connected by massless springs was used to calculate the natural frequencies and mode shapes of the empty Agena (ref. 7) and Thor (ref. 8). Both free-vibration and forced-vibration (without damping) analyses using a continuous model derived by receptance techniques were conducted for the Thor. (See ref. 8.) Results of an experimental study of the longitudinal vibrational response of the Thor having simulated propellants and tank ullage pressures are presented in reference 3. The effects of nonresonant responses of the forced-vibration modes are discussed and the presence of a significant amount of off-resonant vibration when using a single source of vibration excitation is indicated. Experimental studies of the empty Agena and Thor were also conducted and are discussed in references 7 and 8, respectively.

More recently, an experimental and analytical longitudinal vibration study of the combined Thor-Agena two-stage vehicle having simulated propellants has been carried out and the results are presented in the present paper. Emphasis is placed on the use of phase and magnitude measurements and associated results of free- and forced-vibration analyses to further the understanding of the vibrational response of complex structures.

Tests were conducted with both stages empty, and with the second stage full and various amounts of simulated propellants in the first stage.

SYMBOLS

C_{11}, C_{12}, C_{22} orthotropic stress-strain coefficients

C_{33}, C_{34}, C_{44} orthotropic moment-curvature coefficients

f frequency

f_a predicted frequency, Hz

f_e measured frequency, Hz

f_n natural frequency

g acceleration due to gravity, 980.7 cm/sec^2

k stiffness, N/cm

m mass, kg

x displacement, cm

μ damping coefficient

ω circular frequency, rad/sec

$[\,]$ square matrix

$\{\,\}$ column matrix

Subscripts:

1,2,3,4 represents location on structure

APPARATUS AND TEST PROCEDURE

General Description of Test Vehicle

The test vehicle is the structurally complete two-stage launch vehicle shown schematically in figure 1. The first stage is a Thor (DM-18A) and the second stage is an Agena-B. An abbreviated description of the vehicle is presented; however, a more detailed description may be found in references 3 and 7 for the Thor and Agena, respectively.

The total test vehicle length is 21.9 meters. It is cylindrical from station 0 to station 386.0 (diameter of 2.44 meters) and from station 632.0 to station 861.2 (diameter of 1.52 meters). The vehicle tapers virtually linearly between stations 386.0 and 632.0. The dry mass of the test vehicle is 3450 kilograms and, including simulated propellants representing conditions at a flight time near lift-off, the maximum total mass is 36 190 kilograms. Details of the various mass conditions may be found in table I. Some secondary components such as attitude controls and vernier engines were not available for installation and were simulated with mass in the form of lead ballast at various points.

Description of First Stage

The first stage (fig. 2) consists of four basic sections: the engine and accessories section, the liquid-oxygen (oxidizer) tank section, the center-body section, and the fuel-tank section.

Engine and accessories section.- The engine and accessories section (station 0.0 to station 85.3) is approximately 2.17 meters long and has a diameter of 2.44 meters. This section is of semimonocoque construction with circumferential stiffeners. (See fig. 3.) Three thrust beams, constructed of forged and machined fittings and extruded angles and webs, are spaced 120° apart on the wall and extend the length of the section. At the top of these beams are forged thrust fittings that provide the attachment locations for the engine assembly.

The engine assembly consists of a large tripod-shaped thrust frame to which the elements required to operate the engine are attached. The heaviest components are the turbopump, the thrust chamber, and the gimbal block.

Liquid-oxygen (Lox) tank.- The liquid-oxygen tank section (station 85.3 to station 353.0) consists of the propellant tank and the tank skirt. It is approximately 6.80 meters long and has a diameter of 2.44 meters. The interior of the tank is of waffle-pattern construction with ring stiffeners at intervals along its length. The fuel-transfer tunnel extends through the liquid-oxygen tank. The forward and aft bulkheads have an ellipsoidal shape with integrally milled reinforcing stiffeners extending radially.

Center-body section.- The center-body section (station 353.0 to station 386.0) is approximately 0.84 meter long and has a diameter of 2.44 meters. It is of semimonocoque construction and has several cutouts, doors, and hinged panels.

Fuel tank.- The fuel tank (station 386.0 to station 571.0) is approximately 4.7 meters long and its diameter varies from 2.44 meters at its aft end to 1.90 meters at its forward end. The interior of the tank is of waffle-pattern construction with ring stiffeners and fuel-slosh baffles extending around the tank circumference at intervals along its length. The forward and aft bulkheads are ellipsoidal with integrally milled reinforcing stiffeners extending radially. The fuel-transfer-tube attachment is located at the center of the aft bulkhead.

Description of Second Stage

The second-stage vehicle (fig. 4) consists of five basic sections: the transition section, the adapter section, the aft-equipment-rack and engine cone assembly, the propellant tanks, and the forward equipment rack. The overall length of this stage is approximately 7.37 meters.

Transition section.- The transition section (station 571.0 to station 615.0) is a conical frustum approximately 1.12 meters long with a major diameter of 1.90 meters and a minor diameter of 1.62 meters. This section is of semimonocoque construction and consists of aluminum skin, frames, and stringers.

Adapter.- The adapter section (station 615.0 to station 716.0) is a combination of a conical frustum approximately 0.43 meter long and a cylinder approximately 2.13 meters long. The largest diameter of the frustum is 1.62 meters and the smallest diameter is 1.52 meters. The walls of the shells are constructed of magnesium thorium and fastened together in a riveted butt joint strengthened with aluminum straps. Circumferential and longitudinal stiffeners are located on the inside of this section.

Aft-equipment-rack and engine sections.- The aft-equipment-rack section (station 716.0 to station 727.8) is constructed of magnesium and has a total length of 1.78 meters. This section consists of conical frustums and cylinders having circumferential and longitudinal stiffeners. The engine and nozzle assembly attaches to the inside of the aft-equipment rack. The diffusion nozzle was simulated with a lead mass.

Propellant tanks.- The propellant tanks section (station 727.8 to station 810.4) consists of two aluminum tanks separated by a common bulkhead and is approximately 2.10 meters long. All three bulkheads are hemispheres. Propellant-slosh-inhibitors (screens) are located in the lower tank.

Forward equipment rack.- The forward-equipment-rack section (station 810.4 to station 861.2) is constructed of magnesium thorium and is approximately 1.29 meters long.

Two reinforced I-beams are located at the forward end for payload attachment. Numerous panels and stiffeners are located throughout the section.

Propellant simulation.- Simulated propellants were located in each of the four tanks. Water was used to simulate the first-stage fuel and oxidizer whereas, naphtha and freon were used to simulate the second-stage fuel and oxidizer, respectively.

Suspension System

The test vehicle was supported along its longitudinal axis on a low-frequency support system. (See fig. 5.) The system was designed to have a minimum effect on the vibration of the test vehicle while maintaining the vehicle at a fixed predetermined elevation. The use of simulated liquid propellants required that the vehicle be supported in a vertical position. The vehicle was too heavy to be supported directly on the shaker, and the wide range of propellant conditions precluded the use of interchangeable helical springs. A unique, automatically controlled, air-bellows system had been developed to meet the requirements of the suspension system and had been used successfully, as reported in reference 3. A detailed description of the system is given in references 9 and 10.

Instrumentation

The instrumentation was designed to provide data necessary to define the longitudinal resonant frequencies and associated response shapes of the test vehicle. Accelerations were measured on the vehicle shells along the length of the vehicle, on the bulkheads, and on various masses such as the turbopump and engine. Pressure variations at the top and bottom of the propellant tanks and at the bottom of the Thor fuel-transfer tube were measured. Representative strains on the bulkheads and the adapter section were also recorded. The input force to the test vehicle was provided by an electromagnetic vibration exciter and was measured by a force gage located between the shaker and the gimbal thrust pad of the vehicle. A servo-oscillator was used to maintain a predetermined constant level of input force.

The primary transducers were lightweight crystal accelerometers with charge-amplifier signal-conditioning equipment. Pressures were measured by strain-gage-type pressure transducers. The pressure transducers and strain gages used 3-kc-carrier signal conditioning equipment. Data were recorded on a magnetic tape in analog form for subsequent data reduction.

During tests of each configuration, it was necessary to reproduce the data to a suitable form for on-site data interpretation to observe the input and response signals for proper levels and wave shape for computerized data reduction. Oscilloscopes, voltage

meters, and recorders were used to monitor the signals before they were recorded on analog tape.

Experimental Procedure

Longitudinal response data were obtained while applying ±1334 newtons of vertical, sinusoidal force at the first-stage gimbal block. The forcing frequency was varied from 5 to 100 Hz at a constant rate of 0.46 octave/minute (9.4 minutes per sweep). Frequencies at which a peak response was observed from the signal of the input accelerometer along with an associated 90° phase difference or tendency toward 90° phase difference between the input force and input acceleration were defined as resonant frequencies and selected for more detailed study. Amplitude and phase data of all transducers were recorded at small incremental frequencies about the selected frequency to obtain a better definition of the peak response.

Experimental data were obtained for each configuration listed in table I. Masses of the simulated propellants and the pressure present in each tank are also presented in table I.

DATA INTERPRETATION TECHNIQUES

It has long been recognized that, at times, it is difficult to measure normal modes of a complex structure. As discussed in reference 11, for a single normal mode all points on a structure are vibrating either in phase (0°) or out of phase (180°) with respect to each other. Intermediate values of phase angles are not permitted. Since this situation does not always occur during tests of complex structures, the following set of definitions are used in this report to provide clarity. A "natural frequency" is defined as the frequency of a normal mode which satisfies the requirements stated above. "Resonant frequency" is used to identify the frequency of modes indicated by a peak total response in the frequency-sweep test but which do not necessarily satisfy these requirements. Plots of the vehicle response as a function of the vehicle length are called "mode shapes" for natural frequencies and "resonant response shapes" for resonant frequencies. Experimental data and results of the forced-response analysis are resonant frequencies and resonant responses, and results of the free-vibration analysis are natural frequencies and mode shapes.

Two phenomena which may cause the total response of a system at resonance not to represent the true normal mode response are (1) responses at a frequency which is an integral multiple of the excitation frequency, and (2) responses from other modes of the system. In an effort to extract the normal-mode response from experimental data, two data interpretation techniques were utilized to remove the effects of these two causes of

extraneous inputs. A computerized harmonic analysis separated, from the total response, responses at frequencies other than the excitation frequency and a vector component technique was used to separate the normal-mode response from the total response around a resonant frequency.

Computerized Harmonic Analysis

In the first method of data interpretation, a computerized process was used. Data obtained while the vehicle was being excited at a constant frequency were recorded on magnetic tape and were later converted from analog to digital format suitable for computer-mechanized reduction utilizing a 24 points-per-cycle sampling rate of nine consecutive data cycles. These samples were checked for uniformity of wave shape, frequency, and magnitude and then were used to construct a single cycle of data considered to be representative of the set from which it originated. This constructed cycle was then resolved, by using a Fourier series expansion, into the magnitudes of the fundamental frequency (excitation frequency) and the first ten harmonic frequencies. Phase angles and magnitudes relative to various data channels were also calculated for the fundamental frequency component of each response signal.

Resonant frequencies were selected as the frequencies for which the fundamental frequency component of the acceleration measured on the thrust structure at station 30.9 was a peak and the phase angle between this acceleration and the input force was nearly 90° and decreasing in magnitude. Response shapes were determined at each of these frequencies by noting the relationship of response signals from acceleration, pressure, and strain-measuring transducers.

Vector Component Technique

The second method of data interpretation used in this study utilizes both phase and magnitude of response measurements to separate the normal-mode response at a resonant frequency from the total response at that frequency. The vector-response plots were obtained on an $x\text{-}y_1\text{-}y_2$ plotter by utilizing the instrumentation shown schematically in figure 6. A reference frequency signal obtained from the oscillator governing the frequency of the electromagnetic shaker was used as the control signal to a tracking filter and an analog signal proportional to the frequency was used as the input to the y_2-axis of the plotter. The phase angle between the filtered acceleration and force signals was measured and analog signals proportional to these outputs were used as inputs to a sine-cosine resolver. The sine-cosine resolver produced signals proportional to the in-phase and quadrature components of the acceleration response referenced to force. These signals were inputs to the x- and y_1-axes of the plotter. The signals proportional to the

in-phase component and to the excitation frequency were used for correlation between the vector responses and excitation frequency.

The vector-response plots are used to obtain the natural frequency, normal-mode amplitude, and damping of a resonance. This method is discussed in detail in references 11 to 15 and a brief discussion of the technique as applied in this study is presented in appendix A.

ANALYTICAL INVESTIGATION

Computer Program

The analytical program used to compute the longitudinal response of the test vehicle is described in detail in references 16 and 17 and only a brief description is presented herein. The vehicle is assumed to be comprised of three basic types of components: axisymmetric shells having isotropic or orthotropic properties, incompressible and inviscid fluids, and concentrated-masses-and-massless-springs system. Effects of pressure inside of propellant tanks are also included. The stiffness and mass matrices of each shell, spring-mass system, and fluid component are formulated by applying the Rayleigh-Ritz procedure by assuming polynomial displacement functions. The stiffness and mass matrices of the complete launch vehicle are obtained by superposition of the matrices of the individual elements. The natural frequencies and mode shapes are then found from the standard eigenvalue equation $[k]\{x\} - \omega^2[m]\{x\} = 0$ in which $[k]$ and $[m]$ are the stiffness and mass matrices of the vehicle, respectively, ω is the natural frequency, and $\{x\}$ is the modal vector whose elements are the longitudinal, radial, and rotational system coordinate displacements. Applications of the free-vibration part of this analysis applied to a 1/10-scale Apollo-Saturn V model and a 1/5-scale Titan III model are presented in references 18 and 5, respectively.

This program also predicts forced-vibration steady-state responses due to a simple harmonic force. Once these responses are determined, the total displacement response at each coordinate on the launch vehicle is expressed as the linear superposition of the individual modal responses based on an assumed modal damping factor. A modal damping factor of 2 percent of critical damping was assumed for this study.

Formulation of Models

Two analytical models were used to predict the natural frequencies and associated mode shapes of the two-stage vehicle. In one model (fig. 7), both stages were represented by the three basic types of components as discussed. In the second model the second-stage vehicle was represented by a rigid mass concentrated at the top of the first-stage model. This mass represented the total mass of the second stage including simulated

propellants. It should be noted that spring-mass components 1, 3, and 7 are systems cantilevered from shell structures and components 2, 4, 5, and 6 represent circumferential stiffeners and fuel-slosh baffles attached to the shell walls.

Formulation of the analytical models was straightforward but considerable effort was necessary to calculate the required shell stiffness parameters by using the relationships for anisotropic structures presented in references 19 and 20. The constants used in the analytical program were determined either with calculations based on dimensions given on vehicle drawings or dimensions and weights measured from the actual test vehicle structure. Stiffness and mass parameters for the two-stage analytical model are presented in table II.

The spring rates of the two spring-mass components representing the first-stage turbopump and thrust structure and the second-stage engine were based on experimental data. The data presented in reference 7 indicated that the first longitudinal resonant frequency of the second-stage engine was approximately 115 Hz and that the engine mass was 135 kg. When a single degree of freedom system was assumed, the spring rate was calculated to be 0.713×10^6 N/cm. This engine was represented as a single degree of freedom system. (See fig. 7.)

Efforts to obtain an adequate representation of the first-stage turbopump and thrust structure was somewhat more complex. The experimental data (to be discussed later) indicate that two resonant frequencies of the vehicle are related to the turbopump and thrust structure. With various amounts of simulated propellants in all tanks, these frequencies are approximately 45 Hz and 82 Hz. At the lowest frequency mode, the turbopump and thrust structure are responding in phase; in the other mode, the structures are responding out of phase with each other. The frequency sweep data also indicate this trend. The experimentally measured response shapes show that the turbopump always has a response greater than the response of the thrust structure. Based on these observations, the turbopump and thrust structure were mathematically represented as a two-degree-of-freedom spring-mass system (spring-mass system 7, fig. 7). The mathematical spring rates were adjusted so that the lowest frequency of the system was 45 Hz. This adjustment resulted in the highest frequency of the system being 95 Hz.

PRESENTATION AND DISCUSSION OF EXPERIMENTAL RESULTS

The vibration response characteristics of a full-scale two-stage launch vehicle having various amounts of simulated propellants were determined by means of force-controlled vibration techniques. Magnitude and phase of forced vehicle responses, resonant and natural frequencies, resonant response and mode shapes, and damping values were determined for each vehicle configuration under simulated free-free boundary

conditions. In addition, an investigation into the degree of nonresonant vibration contributions to the resonant responses was performed.

Resonant Frequencies and Damping

A summary of resonant frequencies measured for each configuration of the vehicle is presented in table III. A plot of the frequencies of modes having similar response shapes for different configurations is presented in figure 8. These selected resonances have been designated modes A, B, C, D, E, F, and acoustic resonances of the first-stage fuel and oxidizer propellant tanks. Even though a mode was identified for two consecutive configurations, a line was not drawn to connect the two modes unless the frequency of the mode followed the same trend established by other consecutive configurations. For example, mode C was identified for each configuration; however, the trend established by configurations 3 to 8 (that is, constant frequency) was not satisfied by the frequencies measured for configurations 1 and 2. Thus, a line was not drawn between configurations 1 and 2 and between configurations 2 and 3 for this mode.

Additional resonances (designated as other modes in table III) occurred, but trends could not be established because the response shapes were not similar for each configuration.

A decrease in frequency with increasing liquid mass occurs for modes A, B, and E, as would be expected for a dynamic system to which mass was added. The first structural mode (mode A) is a tension-compression bar-type mode and was observed for all configurations. Mode E was not observed during the initial experimental tests since it does not satisfy the previously stated definitions of natural or resonant frequencies; however, by using the results of the analysis as a guide, a review of the measured tank pressures revealed the existence of this mode for configurations 4 to 8.

Mode B was identified for configurations 5 to 8. A further investigation of this mode was conducted by varying the mass of the simulated propellants in the first-stage tanks separately, and measuring the resulting resonant frequency. These data, presented below, indicate that this resonance is dependent on the mass of the simulated oxidizer and independent of the mass of the simulated fuel. Frequency-sweep plots showed no significant change in resonant frequencies of other modes during this limited investigation.

Simulated oxidizer mass, kg	Simulated fuel mass, kg	Mode B resonant frequency, Hz
17 645	9435	25.8
17 645	6485	25.8
12 110	6485	33.8

The resonant frequencies of modes C and D were measured for each configuration. With simulated propellants placed in the first-stage tanks, the resonant frequencies of these modes were measured at 45.5 Hz and 82.5 Hz. Additional amounts of first-stage simulated propellants had a negligible effect on these resonant frequencies. However, with the first-stage tanks empty and the second-stage tanks full the resonant frequencies were 54.5 Hz and 88.0 Hz with both stages empty the resonant frequencies were 61.0 Hz and 88.0 Hz. Mode F was obtained only for configurations having simulated propellants in the second-stage tanks. The resonant frequency of this mode (≈62 Hz) was independent of the mass of the first-stage simulated propellants. The acoustic modes (determined by propellant tank pressures) were measured for all configurations (Table IV) and are dependent only on the distance between the liquid surface and the top bulkhead of the tank in which the liquid was contained.

Resonant frequencies of the two-stage vehicle are compared with those of the first-stage vehicle in appendix B. These data indicate that the addition of the second stage significantly affected the resonant frequencies of mode A for lightweight conditions. No effects were noted for the resonant frequencies of modes B and C.

Frequency Response

Resonant frequencies of the two-stage vehicle were selected from frequency-response plots obtained at several stations along the length of the vehicle. The acceleration response of the thrust frame at station 30.9 (location of applied force) and the relative phase between this acceleration and the applied force are shown for each configuration in figure 9. The frequencies at which resonances were identified and reported are indicated by the appropriate symbols on the acceleration curves. The analytical results presented in this figure are discussed later. The frequency and magnitude of the acceleration response of mode A decreases for heavier mass configurations until for configuration 8 neither a peak response nor a meaningful phase angle was discernible. This mode is very clearly indicated in the phase-angle-response curve for configuration 7 even though only a small acceleration peak was obtained. Modes B and C are normally very clearly indicated by peaks in the acceleration-response curves and by a 90° phase angle in the phase-response curves. Comparison of these response curves with those for the first-stage vehicle (ref. 3) indicates that the addition of the second stage resulted in modes being more evident as peaks in the acceleration-response curves.

In general, the first-stage oxidizer tank acoustic mode is evident as a peak in the acceleration-response curves and a 90° phase angle in the phase-angle-response curves. However, the fuel-tank acoustic mode is considerably less discernible. Unidentifiable resonances are also present in these curves and are designated as other modes.

Vector-response plots of the thrust structure acceleration for several configurations are presented in figure 10 along with a logarithmic-frequency plot for response-frequency correlation. The presence of modes having resonant frequencies below 50 Hz are indicated either by coincidence of peak response and 90^{o} phase, or by inflections or loops in the polar response plots. (See refs. 12 and 13.) In general, the modes are more distinct in these plots than in the separate response and phase plots and at times significant off-resonance response is indicated. Above 50 Hz, the polar-response plots are, in general, not very clear and a further division of the plots for additional and narrower bandwidths of frequency is desirable for meaningful interpretations.

Acceleration-response curves for the turbopump and for stations along the length of the vehicle were also obtained to aid in describing the modes and are presented in figures 11 and 12, respectively. The acceleration response of the turbopump is very similar to that measured on the thrust structure, being very complex and showing many peaks. The important difference between the two structures is shown in the phase-angle curves. When figures 9 and 11 are compared, it is seen that the turbopump is in phase with the thrust structure until about 70 Hz when the first stage is empty (configurations 1 and 2) and until approximately 58 Hz when the first stage is loaded with simulated propellant (configurations 3 to 8). Above these frequencies, the structures appear to respond out of phase throughout the frequency range of the test. The accelerations measured at stations along the length of the vehicle are extremely complex and many of the peak responses are possibly attributable to local structural components and/or panels having resonant frequencies in the immediate frequency range of interest.

Examples of the pressures measured at the top and bottom of the propellant tanks and relative strains measured on bulkheads of the propellant tanks and on the adapter section are presented in figures 13 and 14, respectively, for configuration 3. The acceleration measured at station 30.9 is also shown in this figure for reference. The pressures measured in the propellant tanks have a complex variation consisting of many peaks at the bottom of each tank and only a relatively few peaks occurring in the pressure measured at the top of each tank. These curves were the most valuable means of obtaining the resonant frequencies of the acoustic modes. For this configuration, the fuel and lox tank acoustic modes occur at 36.0 Hz and 30.5 Hz, respectively. The pressure variations in the top of the second-stage propellant tanks were more active than those of the first stage. Calculations analogous to those for the first-stage tanks indicate that the acoustic frequencies of the second-stage propellant tanks are out of the frequency range of interest.

The variations of strain at several locations on the vehicle are shown in figure 14. Each strain gage indicated a large response at the frequency of mode A. However, at

higher frequencies it is extremely difficult to correlate large strain with specific modes. The output of the strain gages located on the bottom bulkhead of both first-stage propellant tanks indicate very complex responses above 30 Hz.

Vector-response plots of the accelerations measured at several stations along the length of the vehicle are presented in figure 15 at frequencies near mode A for configuration 2. "Best circles" drawn through these data indicate that there is some nonresonant response present in the experimentally measured accelerations.

Resonant Response Shapes

Some response shapes of the test vehicle while vibrating at various resonant frequencies are presented in figures 16 to 21 for selected configurations. The arrows located in the sketch of the vehicle indicate the direction of the forces of the simulated liquid-propellant masses on the bottom bulkhead of each tank and the direction of the force generated by the input acceleration. Results obtained by using the computerized technique and comparative results obtained from vector response plots are presented in figure 22.

Response shapes from harmonic analysis of data.- The resonant response shapes for mode A of configurations 1, 2, 3, 5, and 8 are presented in figure 16. This mode is a tension-compression mode having one node and with the cantilevered structures (turbopump, thrust structure, engine, and aft equipment rack) responding in phase with the structure at their respective attachment points. The simulated propellants also respond in phase with the adjacent structure. However, as the mass of the first-stage simulated propellants increases, the node moves from a station near the middle of the first-stage fuel tank (configuration 3) to a station below the fuel tank (configuration 5). The response shapes of mode A were not determined for configurations 7 and 8 because of the limitation of the instrumentation at very low acceleration levels.

Response shapes measured for mode B are presented in figure 17 for configurations 5 and 8. The measured responses indicate a tension-compression mode with the vehicle aft end responding in phase with the thrust structure. The force generated by the simulated fuel is out of phase with the thrust structure and the response of the other simulated propellants change in going from configuration 5 to configuration 8.

The resonant response shapes measured for mode C are presented in figure 18. For configuration 1 the vehicle is responding in a tension-compression mode with the turbopump and thrust structure vibrating in phase with the vehicle at the lower end. It should be noted that the phase relationships between the acceleration responses were not either 0° or 180° as indicated by the response shape. Actually, the measured angles were normally close to 90° or -90° relative to each other (table V). This mode is discussed

further in the section titled "Comparison of Experimental and Analytical Results." In configuration 2 the structure is responding out of phase with the turbopump and thrust structure and the forces generated by the simulated propellants are out of phase with the structure.

For configurations 3 to 8, the response shapes measured for mode D are similar in shape. Basically, the structure is in phase with the input acceleration and the simulated propellants are responding out of phase. Since the resonant frequency and the corresponding response shape do not change with an increase in mass of the simulated propellant, it is believed that this mode is related to a cantilevered spring-mass system having its effective dynamic properties (that is, stiffness, mass, and/or damping) altered when the simulated propellants are initially placed in the first-stage propellant tanks. The relationship of this mode to the thrust structure and turbopump system was initially discussed in reference 3.

In figure 19 the resonant response shapes of mode D are presented for configurations 1, 2, 3, 5, and 8. For the first two configurations the turbopump and thrust structure are vibrating in phase and for configurations 3 to 8 the responses are out of phase with each other. Responses of the simulated propellants, as indicated by pressure measurements, do not follow any definite trend. More discussion of modes C and D may be found in the section dealing with the formulation of the analytical model.

The resonant response shapes of mode F are presented in figure 20 for configurations 2, 3, 5, and 8. This mode was present only for configurations having simulated propellant in the second-stage tanks. With first-stage tanks empty, the vehicle responds out of phase with the thrust structure and turbopump and the second-stage simulated propellants respond out of phase relative to each other. For configurations 3 and 5, all the structures, including the cantilevered components, vibrate in phase relative to each other and the simulated propellants generate forces out of phase with the structure. For configuration 8 the first-stage simulated oxidizer is responding out of phase with the other simulated propellants.

Table III lists the frequencies measured for modes which could not be associated with any other modes because of a lack of commonality between response shapes. The associated response shapes are presented in figure 21 except for the apparent resonance occurring at 24.5 Hz for configuration 1. This mode is hypothesized to be related to lateral motions within the aft-equipment-rack and engine sections of the second stage. The primary function of the instrumentation was to measure and identify longitudinal responses and sufficient lateral response data are not available to identify all responses. However, significant observations which tend to support this hypothesis are:

(1) It was reported in reference 21 that the aft equipment rack has lateral resonant frequencies near 20 Hz,

(2) In the present investigation instrumentation indicated significant lateral response in aft-equipment-rack and engine structures and,

(3) All measured longitudinal responses are in phase and thus are not satisfying the conservation of momentum principle for vibrating structures.

Comparison of data interpretation methods.- Structural response shapes of mode A of configurations 2 and 3 obtained by using the two methods of data interpretation are presented for comparison in figure 22 with resulting good agreement for both response shapes and resonant frequencies. In addition, reasonably good agreements were obtained for all modes of the investigation having resonant frequencies below 50 Hz. As discussed previously, above this frequency, the polar response plots are not very clear and accurate data interpretation is not possible. It should be noted that although the best circles (see appendix A) showed that the normal mode amplitude is different from the experimentally measured amplitude, normalization of the data gives good correlation between the two data interpretation methods. These results indicate that the influence of off-resonant response on a mode is similar at each station along the length of the vehicle.

The damped natural frequencies and damping factors obtained from vector-response plots are given in table VI. The frequencies are in good agreement with those determined during constant-frequency tests. The damping factors of the modes varied considerably for different configurations and ranged from $\mu = 0.028$ for mode B of configuration 6 to $\mu = 0.0086$ for mode C of configuration 3. In general, these factors are lower than those previously determined for the one-stage vehicle (ref. 3).

COMPARISON OF EXPERIMENTAL AND ANALYTICAL RESULTS

Free-vibration and forced-vibration analyses, using a two-dimensional finite-element model, of the two-stage vehicle were conducted and the results are compared with each other and with the experimental data in this section. The natural frequencies and the associated mode shapes predicted by the free-vibration analysis are presented with the corresponding experimental data in table III and in figures 16 to 21. The identical analytical model used in the free-vibration analysis was used to obtain forced-vibration results. The steady-state forced responses were obtained from a linear superposition of the free-vibration modes based on an assumed modal damping of 2 percent of critical damping. Plots of responses against frequency are presented for the thrust structure, turbopump, and selected stations along the length of the vehicle in figures 9, 11, and 12, respectively. Best circles have been drawn through the predicted accelerations for modes A and E of configuration 5 and are presented in figure 23. Typical normalized responses obtained from free-vibration analysis, interpretation of vector-response plots, and from magnitudes of forced responses at the natural frequencies predicted by the

free-vibration analysis are presented in tables V and VII. Table II presents the experimentally obtained acoustic resonant frequencies in the air column above the simulated propellants in the first-stage tanks and the acoustic resonant frequencies calculated by using the frequency equation for the vibration of an air column (ref. 22).

Comparison of Experimental Data With Free-Vibration Analysis

Natural frequencies.- The natural frequencies predicted by the free-vibration analysis are, in general, in good agreement with the experimentally measured resonant frequencies. In table III the analytical results were obtained with the mathematical model having both stages and their components represented by shells, springs, and masses. The predicted frequency of the first mode (mode A) is higher than the measured frequency for configurations 1 to 5 and lower for configurations 6 to 8. The predicted frequency for mode B was always greater than the measured frequency. For configuration 5 the analysis predicted that this mode would occur at a frequency greater than that for mode C. Actually, the mode has a frequency less than the frequency of mode C. This lack of agreement may, in part, be attributed to the occurrence of four modes, within a frequency range of 6 Hz (that is, between 38.8 Hz and 44.8 Hz). The natural frequencies predicted for modes C and D are in good agreement with the measured frequencies. The good agreement was obtained only after experimental data indicated the numerical value of their resonant frequencies. The frequencies predicted for mode D are slightly higher than the experimental frequencies for all configurations. This result was expected since the higher frequency of the two-degree-of-freedom system representing the turbopump and thrust structure in the analytical model is 95.2 Hz. This representation is discussed in more detail in the section on the formulation of the analytical model. The predicted frequencies for mode E are in better agreement with the measured frequencies for the heavier configurations. It should be noted that the experimental frequencies for mode E were obtained only after the analysis indicated their presence and a review of the experimental data revealed that previously undetected peaks occurred in the pressure measurements in the first-stage fuel tank near the predicted frequencies.

Agreement was obtained between the experimental and analytical frequencies of mode F for each configuration only after changing in the mathematical model the height of the fluid in the lower tank of the second-stage vehicle so that this fluid did not touch the common bulkhead. The mass of this fluid was kept constant by increasing the fluid density. Further reduction of this fluid height had a significant effect on the predicted mode shapes of mode F but little effect on the predicted frequencies. This phenomenon points out the need for an analytical procedure which can properly represent the propellant-bulkhead interaction of tanks with a common bulkhead.

A brief free-vibration study was conducted to determine whether an adequate analytical model of the two-stage vehicle could be formulated by representing the second-stage vehicle as a rigid mass attached to the forward end of the original model of the first-stage vehicle. This study is presented in appendix B and results indicated that the analysis using the simplified model did predict the measured modes below 60 Hz satisfactorily.

Mode shapes.- The mode shapes predicted by the analytical model of the two-stage vehicle are plotted with the experimental data for configurations 1, 2, 3, 5, and 8 in figures 16 to 19. In most cases the predicted and measured mode shapes are in good agreement. For mode A excellent agreement was obtained. The analysis shows that for this mode the relative phase of the motion of the propellant in the first-stage fuel tank changes 180° between the lighter and the heavier weight conditions and always responds in phase with the associated structure.

Excellent agreement between the normalized measured and predicted response shapes was also obtained for mode B as shown in figure 17 for configuration 8. Although not shown herein, similar correlation was obtained for configurations 6 and 7. The response of the structure is similar to that measured for mode A; however, the response of the simulated oxidizer propellant is out of phase with the associated load-carrying structure. The predicted mode shape of mode C varied significantly with simulated propellant mass. (See fig. 18.) Experimentally, the normalized response shapes were similar for configurations 3 to 8. The agreement between the predicted and measured responses was excellent for configurations 5 to 8 and only fair for configurations 2, 3, and 4. As previously discussed for configuration 1, abnormal phase data were measured for this mode. The predicted free-vibration responses (eigenvectors) are presented in table V for correlation with the measured responses. The agreement between the predicted and measured response shapes is poor.

The predicted and measured response shapes for mode D are in fair agreement for configurations 3 to 8. (See fig. 19.) The most apparent difference is in the phase relationship of the simulated propellants responses. In each of these configurations, the turbopump response is out of phase with the input acceleration. For the configurations in which the first-stage propellant tanks are empty (configurations 1 and 2), the analysis predicts that the first-stage turbopump would respond out of phase with the thrust structure. This response did not occur experimentally.

The mode shape predicted for mode E is shown in figure 17 for configurations 3, 5, and 8. As previously mentioned, mode E was not investigated during the experimental part of the program.

Modes other than those discussed were predicted in the frequency range of interest (less than 100 Hz) but they did not follow any definite trend and comparison of response

shapes did not indicate any specific correlations. Response shapes of these modes for configurations 5 and 8 are presented in figure 24.

Comparison of Experimental Data With Forced-Vibration Analysis

Frequency response.- The predicted amplitude and phase responses of the thrust structure at the location of the input force of 1334 newtons (station 30.9) are presented in figure 9 with the experimental data for each configuration. Good agreement was obtained below 60 Hz except in the frequency range of the acoustic modes which were not considered in the analytical model. For mode A the analysis accurately predicted the experimentally observed decrease in amplitude and the lesser tendency of the phase angle to change completely from 180° to 0° as the mass of the simulated propellants was increased. The analytical results presented in figure 9 show that there is no peak acceleration value of the thrust structure response and only a slight change in the associated phase response for mode E; thus, this mode would be difficult to obtain experimentally. Around 60 Hz (mode F), the agreement is poor. The analysis indicates a dip in the acceleration and the experiment indicates a peak acceleration. Between 60 and 85 Hz, the trend of the predicted responses agrees with experimental data but above 85 Hz, the agreement between the predicted and measured phase is again poor.

The predicted amplitude and phase responses of the turbopump are presented in figure 11 with the associated experimental data for each configuration. The predicted accelerations are in good agreement with the experimental data for all configurations. The predicted phase responses are in good agreement with the experimental data up to approximately 60 Hz. The trend agreement is good up to approximately 85 Hz.

The correlation between the predicted and measured responses along the length of the vehicle is fair for modes A (19.6 Hz) and C (45.5 Hz) of configuration 3 (fig. 12). At other frequencies the predicted responses are much lower than those measured.

Resonant response.- Normalized forced-response data at resonant frequencies are presented in table VII for modes A, C, D, and E of configuration 5. The eigenvectors predicted with free-vibration analysis of the analytical model (see fig. 7) are also given for comparison. The eigenvectors and forced responses are presented for the wall of the vehicle (coordinates 1 to 20), thrust structure (coordinate 37), turbopump (coordinate 38), second-stage engine (coordinate 29), and the aft equipment rack (coordinate 30). The data presented in the forced-response column of table VII were obtained from the forced-response analysis at the natural frequency predicted by the free-vibration analysis. Data were also obtained from polar plots of acceleration vectors (for example, fig. 23) for arbitrarily chosen coordinates.

The agreement in the amplitudes determined from the results for the forced responses, polar plot responses, and the eigenvectors of mode A indicates that there is

little coupling between modes at the mode A resonant frequencies and that the small modal damping factor used in the forced analysis had little effect on the relative amplitudes of the structure or on the natural frequencies of the mode A responses. Similar correlations were obtained for mode C.

For mode D the vector-response plots showed some off-resonance contributions; however, the normalized-response shapes obtained from these plots are in good agreement with the forced-response and eigenvector data (table VII). This result indicates that the off-resonant vibrations contribute a constant percentage to the total response measured at each location.

The data presented in table VII for mode E has been normalized to the acceleration predicted for coordinate 20 rather than for coordinate 37. This normalization was necessary since it was not possible to draw a circle in the vector plot of the response predicted for coordinate 37 in the frequency range of mode E. The agreement between the analytical response shapes is poor. This condition may be caused by the considerable amount of coupling present in this mode as indicated in the polar plots of the acceleration vectors. (See fig. 23(b).) This mode was not observed experimentally. (See section entitled "Presentation and Discussion of Experimental Results.")

CONCLUSIONS

An analytical and experimental program has been conducted to investigate the longitudinal vibration properties of a representative two-stage full-scale launch vehicle with simulated propellant loadings and representing various flight times. A two-dimensional finite-element mathematical model of the vehicle was formulated and used as the basis for free- and forced-vibration analyses. Analytical and experimental data were used to investigate a technique of obtaining normal modes and natural frequencies from coupled responses of complex structures. The effects of the presence of the second-stage vehicle on the resonant frequencies primarily associated with the first-stage vehicle are also discussed. Conclusions from the combined analytical and experimental program may be summarized as follows:

1. Concurrent use of phase and magnitude of experimental and analytical responses provided an efficient and accurate means of obtaining the resonant frequencies and response shapes of a complex full-scale two-stage launch vehicle having simulated propellants. Results from vector-response plots of the experimental data agreed well with results from the harmonic analysis of peak-response experimental data.

2. Vector-response plots provided the most practical means of acquiring damping data. Modal damping of the vehicle ranged from 1.4 percent to 0.4 percent of critical damping.

3. A forced-vibration analysis was useful in describing the relative importance and prominence of various modes. This type of analysis predicted the magnitude and phase of the vehicle responses associated with each mode and thus aided in interpreting the experimental data.

4. The analysis accurately predicted the resonant frequencies and response shapes of the vehicle for all weight conditions. However, experimental data were necessary to obtain adequate representations of such primary components as the turbopump and thrust structure. The following type of modes were measured experimentally and calculated: a bar-type structural mode (mode A), three modes related to the simulated propellants (modes B, E, and F), and two modes of spring-mass systems (modes C and D).

5. These data also pointed out the need for (1) the formulation of a mathematical model which can accurately predict the response shapes of a resonance caused by propellants located in tanks having a common bulkhead and (2) a means of experimentally measuring the motions of propellants in launch vehicle tanks.

6. The presence of the second stage attached to the forward end of the first stage reduced the frequencies of the first structural mode (mode A). No similar effect was noted for a spring-mass system mode (mode C), for the mode related to the simulated oxidizer of the first stage (mode B) and for the acoustic modes.

7. Proper identification and correlation of the modes required measurements of accelerations along the length of the vehicle, accelerations of specific components such as engines and turbopumps, and pressures at the top and bottom of the propellant tanks.

8. Acoustic modes in the first-stage propellant tanks caused significant acceleration response of the vehicle with small amounts of simulated propellant. These modes depend only on the distance between the liquid surface and the upper bulkhead.

9. This program has reaffirmed the need for closely related, simultaneously conducted, analytical and experimental studies when investigating the vibration characteristics of a complex system.

Langley Research Center,
National Aeronautics and Space Administration,
Hampton, Va., June 9, 1970.

APPENDIX A

DATA INTERPRETATION UTILIZING VECTOR-RESPONSE PLOTS

A typical vector-response plot (Kennedy-Pancu plots) at a resonance for a system having more than one degree of freedom is shown in figure 25 (taken from ref. 15). The circles represent experimental data, for equal increments of frequency, through which a best circle has been drawn. A best circle is defined as the circle which best follows the trend of the experimental data in the vicinity of the maximum response. A diameter of the circle (JH) drawn perpendicular to the force phase reference (in-phase axis) should pass through the point at which the maximum change in the length of the circular arc with respect to a change in frequency (maximum frequency spacing) occurs. The intersection of this diameter and the circle (point H) locates the resonant frequency and the opposite end of the diameter (point J) locates the displaced origin. The modal response (normal mode component) is given by the length of the diameter (JH). The distance between the displaced origin and the actual origin (OJ) represents the off-resonant contribution. Modal damping is determined from the vector-response plot by means of the method discussed in reference 3. The damping factor μ is calculated from $\mu = \frac{2}{f_n \frac{\Delta\theta}{\Delta f}}$ where μ is twice the ratio of damping to critical damping for an equivalent viscous damped system, $\Delta\theta/\Delta f$ is the slope of the response phase angle in radians with respect to frequency in hertz at the resonant frequency determined from the best circle, and f_n is the resonant frequency in hertz.

An analytical investigation of this technique applied to a two-degree-of-freedom system consisting of a translational spring, a torsional spring, and a rigid flat plate is presented in reference 15. It was shown that for modes in which the off-resonant vibration is not negligible, the modal amplitude measurements using the Kennedy-Pancu technique were much closer to the normal-mode amplitudes than the peak-response amplitudes were. Damping and several modes having nearly identical resonant frequencies significantly affected the accuracy of the Kennedy-Pancu technique.

Although this technique is very useful in separating normal modes, it requires considerable effort to obtain discrete frequency plots for each system coordinate necessary to obtain a complete mode shape for each resonant frequency. The basic concepts of this approach were utilized in the program discussed herein. However, instead of plotting the data for discrete frequencies, vector-response plots were obtained during frequency-sweep tests. Thus, continuous plots were obtained instead of plots having discrete-frequency data points. Much less effort and time were required to obtain the continuous data.

APPENDIX A

As an example, data obtained for the resonance associated with mode A on configuration 2 are presented in figure 26. The vector-response plot in the upper part of the figure shows the total response amplitude of the input acceleration and its phase relative to the input force (real axis). In the lower portion of the figure is shown the real part of the total response as a function of the excitation frequency. These plots were obtained simultaneously so that a correlation between the vector-response plot and frequency could be made. In other words, the frequency at any point on the vector-response plot may be obtained by projecting the point down to the lower trace and reading the corresponding frequency. A best circle was fitted to the data and this fitting resulted in the normal mode response being represented by the diameter JH and the nonresonant response being represented by the distance OJ. The two additional parameters required to determine model damping, $\Delta\theta$ and ΔF, are obtained by selecting a value of Δf at resonance and projecting between the lower plot and the response curve in the upper plot. The change in the angle of response is then measured and a damping value calculated.

APPENDIX B

COMPARISON OF RESONANT FREQUENCIES OF THE TWO-STAGE AND ONE-STAGE VEHICLES

Resonant frequencies of the isolated first-stage vehicle (ref. 3) are presented in figure 27 with comparative data for the two-stage vehicle. Similar modes were obtained for each vehicle and are given the same identification (modes A, B, and C). The total mass of the first-stage vehicle, including simulated propellant loadings in the first-stage tanks, is used as the common factor for means of comparisons.

The resonant frequencies of mode A for the two-stage vehicle are always less than those for the one-stage vehicle. The curves drawn through the experimental data for mode A of each vehicle have the same trend and seem to approach each other asymptotically as the mass of the first stage increases. Thus it appears that the second stage has a significant effect on mode A and this effect decreases as the mass of the second stage becomes a smaller percentage of the total mass of the two-stage vehicle.

The frequencies of modes B and C are primarily dependent on the first-stage simulated oxidizer and the first-stage turbopump-thrust structure, respectively. As would be expected the addition of the second-stage vehicle has virtually no effect on the resonant frequencies of either mode.

Since most of the resonances measured for the two-stage vehicle are similar to those measured for the isolated first-stage vehicle (see fig. 27 for comparison), a brief analytical study was conducted to determine whether an adequate mathematical model of the two-stage vehicle could be formulated by representing the second-stage vehicle as a rigid mass attached to the forward end of the original mathematical model of the first-stage vehicle. The frequencies for modes A, B, C, and E are presented in the following table:

	Mode A	Mode E	Mode B	Mode C
Experimental	13.5	18.5	29.7	46.5
Predicted:				
One stage with mass	13.2	23.0	35.4	44.4
Two stage	12.9	20.4	34.9	44.4

These data show that the analytical model having the second stage represented as a mass does predict the modes of the two-stage vehicle below 50 Hz. Both analytical models predict additional higher frequency resonances, but correlation of the mode shapes is impossible because of the representation of the second-stage vehicle as a concentrated mass in the one-stage mathematical model.

REFERENCES

1. Leadbetter, Sumner A.; Alley, Vernon L., Jr.; Herr, Robert W.; and Gerringer, A. Harper: An Experimental and Analytical Investigation of the Natural Frequencies and Mode Shapes of a Four-Stage Solid-Propellant Rocket Vehicle. NASA TN D-1354, 1962.

2. Peele, Ellwood L.; Thompson, William M., Jr.; and Pusey, Christine G.: A Theoretical and Experimental Investigation of the Three-Dimensional Vibration Characteristics of a Scaled Model of an Asymmetrical Launch Vehicle. NASA TN D-4707, 1968.

3. Schoenster, James A.; and Clary, Robert R.: Experimental Investigation of the Longitudinal Vibration of a Representative Launch Vehicle With Simulated Propellants. NASA TN D-4502, 1968.

4. Mixson, John S.; and Catherine, John J.: Comparison of Experimental Vibration Characteristics Obtained From a 1/5-Scale Model and From a Full-Scale Saturn SA-1. NASA TN D-2215, 1964.

5. Thompson, William M., Jr.: An Investigation of the Response of a Scaled Model of a Liquid-Propellant Multistage Launch Vehicle to Longitudinal Excitation. NASA TN D-3975, 1967.

6. Pinson, Larry D.; and Leonard, H. Wayne: Longitudinal Vibration Characteristics of 1/10-Scale Apollo/Saturn V Replica Model. NASA TN D-5159, 1969.

7. Clary, Robert R.: An Analytical and Experimental Investigation of the Longitudinal Vibrational Response of an Empty and Unpressurized Agena-B Vehicle. M.S. Thesis, Virginia Polytech. Inst., 1966.

8. Carden, Huey D.; and Raney, John P.: An Experimental and Analytical Study of the Longitudinal Vibration of a Simplified Thor Vehicle Structure. NASA TN D-3632, 1966.

9. Schoenster, James A.; Pearson, Jerome; and Dixon, Grayson V.: A Unique Suspension System for Longitudinal Vibration Testing of Large Launch Vehicles. Shock Vib. Bull., Bull. 35, Pt. 2, U.S. Dept. Defense, Jan. 1966, pp. 191-196.

10. Dixon, Grayson V.; and Pearson, Jerome: Automatically Controlled Air Spring Suspension System for Vibration Testing. NASA TN D-3891, 1967.

11. Keller, Anton C.: Vector Component Techniques: A Modern Way To Measure Modes. Sound Vib., vol. 3, no. 3, Mar. 1969, pp. 18-26.

12. Kennedy, Charles C.; and Pancu, C. D. P.: Use of Vectors in Vibration Measurement and Analysis. J. Aeron. Sci., vol. 14, no. 11, Nov. 1947, pp. 603-625.

13. Pendered, J. W.: Theoretical Investigation into the Effects of Close Natural Frequencies in Resonance Testing. J. Mech. Engr. Sci., vol. 7, no. 4, Dec. 1965, pp. 372-379.

14. Bishop, R. E. D.; and Gladwell, G. M. L.: An Investigation Into the Theory of Resonance Testing. Phil. Trans. Roy. Soc. London, ser. A, vol. 255, no. 1055, Jan. 17, 1963, pp. 241-280.

15. Turner, Lloyd J., Jr.: An Analytical Investigation of a Vector Technique for Determining Normal Mode Amplitudes From Vibration Data. M.S. Thesis, Virginia Polytech. Inst., 1968.

16. Archer, J. S.; and Rubin, C. P.: Improved Analytic Longitudinal Response Analysis for Axisymmetric Launch Vehicles. Vol. I – Linear Analytic Model. NASA CR-345, 1965.

17. Rubin, C. P.; and Wang, T. T.: Improved Analytic Longitudinal Response Analysis for Axisymmetric Launch Vehicles. Vol. II – Computer Program Description. NASA CR-346, 1965.

18. Pinson, Larry D.: Evaluation of a Finite-Element Analysis for Longitudinal Vibrations of Liquid-Propellant Launch Vehicles. NASA TN D-5803, 1970.

19. Flügge, Wilhelm: Stresses in Shells. Second Printing, Springer-Verlag, 1962.

20. Dow, Norris F.; Libove, Charles; and Hubka, Ralph E.: Formulas for the Elastic Constants of Plates With Integral Waffle-Like Stiffening. NACA Rep. 1195, 1954. (Supersedes NACA RM L53E13a.)

21. Albert, R. S.: Agena Tank Modal Test. Rept. No. SS/788/5522 (Contract AF04(695)-191), Lockheed Missiles & Space Co., July 17, 1964. (Available from DDC as AD 461821.)

22. Hausmann, Erich; and Slack, Edgar P.: Physics. Fourth ed., D. Van Nostrand Co., Inc., c.1957.

TABLE I.- VEHICLE CONFIGURATION DATA

Configuration	Vehicle mass, kg	First-stage propellant tanks				Second-stage propellant tanks				Total mass, kg
		Simulated oxidizer		Simulated fuel		Simulated oxidizer		Simulated fuel		
		Mass, kg	Pressure, N/cm^2	Mass, kg	Pressure, N/cm^2	Mass, kg	Pressure, N/cm^2	Mass, kg	Pressure, N/cm^2	
1	3450	-----	---	----	---	----	---	----	---	3 450
2	3450	-----	---	----	---	3970	16.2	1690	19.0	9 110
3	3450	2 690	10.4	1440	8.5	3970	16.2	1690	19.0	13 240
4	3450	6 740	10.4	3660	8.5	3970	16.2	1690	19.0	19 510
5	3450	9 370	10.4	5070	8.5	3970	16.2	1690	19.0	23 550
6	3450	12 110	10.4	6485	8.5	3970	16.2	1690	19.0	27 705
7	3450	14 650	10.4	7815	8.5	3970	16.2	1690	19.0	31 575
8	3450	17 645	10.4	9435	8.5	3970	16.2	1690	19.0	36 190

TABLE II.- STIFFNESS AND MASS PARAMETERS OF ANALYTICAL MODEL

[Numbers in parentheses indicate components used in mathematical model]

Shell	Shell stiffness coefficients																		Masses, kg		
	$(C_{11})_1$, MN/m	$(C_{11})_2$, MN/m	$(C_{12})_1$, MN/m	$(C_{12})_2$, MN/m	$(C_{22})_1$, MN/m	$(C_{22})_2$, MN/m	$(C_{33})_1$, N-m	$(C_{33})_2$, N-m	$(C_{33})_3$, N-m	$(C_{33})_4$, N-m	$(C_{34})_1$, N-m	$(C_{34})_2$, N-m	$(C_{34})_3$, N-m	$(C_{34})_4$, N-m	$(C_{44})_1$, N-m	$(C_{44})_2$, N-m	$(C_{44})_3$, N-m	$(C_{44})_4$, N-m	Shell	Concentrated	
1	137.0	137.0	41.0	41.0	139.4	139.4	89.3	89.3	89.3	89.3	26.8	26.8	26.8	26.8	18 500	18 500	18 500	18 500	88.9	(23)	180.0
2	154.0	154.0	46.2	46.2	154.0	154.0	53.1	53.1	53.1	53.1	15.9	15.9	15.9	15.9	53.1	53.1	53.1	53.1	18.2		
3	192.7	192.7	57.8	57.8	192.7	192.7	10.4	10.4	10.4	10.4	31.1	31.1	31.1	31.1	104	104	104	104	8.2		
4	157.8	157.8	47.3	47.3	157.8	157.8	57.2	57.2	57.2	57.2	17.2	17.2	17.2	17.2	57.2	57.2	57.2	57.2	22.2		
5	192.7	192.7	57.8	57.8	192.7	192.7	104.0	104.0	104.0	104.0	31.1	31.1	31.1	31.1	104	104	104	104	54.7		
6	161.7	161.7	48.5	48.5	161.7	161.7	61.5	61.5	61.5	61.5	18.4	18.4	18.4	18.4	61.5	61.5	61.5	61.5	36.9		
7	180.6	180.6	54.1	54.1	180.6	180.6	204	204	204	204	61.4	61.4	61.4	61.4	204	204	204	204	4.6		
8	106.8	106.8	32.0	32.0	106.8	106.8	9 360	468	28.2	28.2	8.48	8.48	8.48	8.48	28.2	28.2	28.2	28.2	27.4	(29)	77.1
9	201.4	201.4	60.4	60.4	201.4	201.4	285	285	285	285	85.4	85.4	85.4	85.4	285	285	285	285	106.2		
10	46.6	46.6	14.2	14.2	39.1	39.1	21 400	21 400	21 400	21 400	6410	6410	6410	6410	8 930	8 930	8 930	8 930	52.8	(30)	135.9
11	155.5	155.5	46.6	46.6	155.5	155.5	131	131	131	131	39.3	39.3	39.3	39.3	131	131	131	131	26.4		
12	259.2	262.7	77.8	78.8	269.7	269.7	676	695	731	765	60.6	60.6	60.6	60.6	7 290	7 290	7 290	7 290	147.7		
13	61.6	481.7	18.4	144.5	61.6	481.7	3.40	3.40	3.40	3.40	1.02	1.02	1.02	485	3.40	3.40	3.40	1 620	25.1		
14	132.6	132.6	45.7	45.7	132.6	132.6	89.7	89.7	89.7	89.7	31.0	31.0	31.0	31.0	89.7	89.7	89.7	89.7	321.1	(10) (11)	12.6 12.6
15	80.9	481.7	24.3	144.5	80.9	481.7	7.68	7.68	7.68	7.68	2.30	2.30	2.30	485	2.30	2.30	2.30	485	38.2	(32)	42.1
16	225.6	225.6	36.4	36.4	121.4	121.4	33 800	33 800	33 800	33 800	7.77	7.77	7.77	7.77	25.9	25.9	25.9	25.9	148.0		
17	80.9	481.7	24.3	144.5	80.9	481.7	7.68	7.68	7.68	7.68	2.30	2.30	2.30	485	7.68	7.68	7.68	1 620	60.4		
18	108.1	108.1	37.8	37.8	108.1	108.1	96.7	96.7	96.7	96.7	33.8	33.8	33.8	33.8	96.7	96.7	96.7	96.7	369.4		
19	96.2	481.7	14.4	28.9	96.2	481.7	12.9	12.9	12.9	12.9	3.88	3.88	3.88	485	12.9	12.9	12.9	1 620	58.5		
20	204.9	204.9	28.9	28.9	134.0	134.0	37 400	37 400	37 400	37 400	38.8	38.8	38.8	38.8	51 000	51 000	51 000	51 000	240.4		
21	225.6	243.1	23.1	23.1	122.4	122.4	425 000	910 000	1 820 000	3 400 000	1.99	1.99	1.99	1.99	497 000	497 000	497 000	497 000	475.3	(37) (38)	408.1 251.9

TABLE III.- PREDICTED AND MEASURED FREQUENCIES FOR TEST VEHICLE

Mode	Configuration 1		Configuration 2		Configuration 3		Configuration 4		Configuration 5		Configuration 6		Configuration 7		Configuration 8	
	Experimental	Analytical	Experimental	Analytical	Experimental	Analytical	Experimental	Analytical	Experimental	Analytical	Experimental	Analytical	Experimental	Analytical	Experimental	Analytical
A	37.5	40.1	26.5	28.3	19.6	21.4	17.0	17.4	15.5	15.7	14.4	14.2	13.5	12.9	12.5	11.6
B	---	---	---	---	---	---	---	---	38.8	52.9	33.8	38.1	29.7	34.9	25.8	31.2
C	61.0	62.7	54.5	56.6	45.5	46.0	45.0	43.1	44.8	41.0	44.5	47.3	46.5	44.4	45.2	41.9
D	88.0	96.0	88.0	91.4	82.5	87.0	81.5	88.9	80.2	89.1	82.5	87.4	82.5	89.2	83.0	87.3
E	---	---	---	---	---	49.4	26.0	31.4	22.5	25.9	20.0	22.4	18.5	20.4	17.0	18.7
F	---	---	63.5	61.6	62.5	61.6	61.5	61.6	61.5	61.6	61.5	61.5	62.5	61.6	61.3	61.6
Other															40.0	---
									53.6	---					42.4	---
	24.5	---	---	---	49.5	---	---	63.4	---	70.4	40.8	---	---	55.3	---	50.1
							---	83.8	---	80.5	58.0	---	---	60.4	---	53.9
											---	62.0	---	82.9	---	70.3
											---	68.1			---	77.8

TABLE IV.- ACOUSTIC FREQUENCIES IN FIRST-STAGE PROPELLANT TANKS

Configuration	Liquid oxygen tank		Fuel tank	
	Calculated frequency, Hz	Experimental frequency, Hz	Calculated frequency, Hz	Experimental frequency, Hz
1	28.3	28.5	35.6	34.0
2	28.3	28.5	35.6	34.0
3	30.6	30.7	36.8	37.0
4	36.4	36.5	41.2	41.0
5	41.5	41.3	44.9	45.0
6	48.5	47.5	49.6	49.0
7	57.9	57.5	55.0	55.0
8	75.0	74.0	64.1	63.0

TABLE V.- MEASURED AND PREDICTED RESPONSES FOR MODE C OF CONFIGURATION 1

Station	Normalized acceleration			Phase angle relative to input acceleration, deg	
	Experimental (61.0 Hz)	Analytical (62.7 Hz)		Experimental from harmonic analysis (61.0 Hz)	Analytical (62.7 Hz)
		Eigenvector	Forced response		
861.2	1.47	-29.8	7.13	97.42	103.7
716.0	.88	-24.2	5.86	106.16	104.3
627.0	.48	-----	----	157.14	----
615.0	.53	-12.9	3.17	181.59	107.0
524.8	---	-3.4	.89	-----	121.5
509.0	1.02	-----	----	110.82	----
478.5	---	2.7	.71	-----	103.6
447.0	1.34	-----	----	86.29	----
432.2	---	8.4	2.06	-----	86.7
386.0	1.58	13.7	3.33	93.59	83.3
353.0	1.68	15.5	3.65	76.89	82.6
306.3	---	20.4	4.91	-----	81.0
295.0	1.63	-----	----	78.88	----
259.6	---	24.9	6.02	-----	80.0
232.0	1.66	-----	----	70.78	----
212.9	---	29.0	6.97	-----	79.3
179.0	1.66	-----	----	78.92	----
166.2	---	32.5	7.77	-----	78.7
119.5	1.57	35.5	8.56	72.82	78.2
85.3	1.59	35.8	8.56	82.22	78.0
85.3	1.84	-----	8.56	59.79	78.0
43.1	.87	-----	----	6.13	----
Thrust structure	1.00	1.00	1.00	0	0
0	---	38.1	9.19	-----	78.1
Turbopump	1.66	-71.9	26.94	50.39	108.9

TABLE VI.- DAMPED NATURAL FREQUENCIES AND DAMPING FACTORS

OBTAINED FROM VECTOR-RESPONSE PLOTS

Mode	Configuration 2		Configuration 3		Configuration 4		Configuration 5	
	Frequency, Hz	Damping, μ	Frequency, Hz	Damping, μ	Frequency, Hz	Damping, μ	Frequency, Hz	Damping, μ
A	26.4	0.021	19.7	0.012	---	-----	---	----
B	---	----	---	-----	---	----	38.4	0.018
C	---	----	45.3	.0086	44.5	0.012	44.4	.010

Mode	Configuration 6		Configuration 7		Configuration 8	
	Frequency, Hz	Damping, μ	Frequency, Hz	Damping, μ	Frequency, Hz	Damping, μ
A	---	----	---	----	---	----
B	33.0	0.028	29.5	0.018	25.7	0.021
C	47.6	.012	46.5	.024	45.4	.028

TABLE VII.- PREDICTED RESPONSES FOR SOME RESONANCES OF CONFIGURATION 5

Coordinate number	Station	Mode A: f_a = 15.7 Hz			Mode C: f_a = 41.0 Hz			Mode D: f_a = 89.1 Hz			Mode E: f_a = 25.9 Hz		
		Eigenvector	Forced response μ = 0.02	Vector response	Eigenvector	Forced response μ = 0.02	Vector response	Eigenvector	Forced response μ = 0.02	Vector response	Eigenvector	Forced response μ = 0.02	Vector response
1	861.2	-2.03	-1.95	-2.12	-0.0104	-0.0105	-0.0189	-0.00147	-0.00159	-0.00175	-5.77	-3.48	-17.0
2	805.0	-2.03	-1.95	----	-.0103	-.0103	-------	-.00138	-.00149	-------	-5.75	-3.45	-----
3	795.2	-2.03	-1.95	----	-.0103	-.0103	-------	-.00104	-.00114	-------	-5.75	-3.45	-----
4	733.4	-1.96	-1.86	-2.12	-.00732	-.00741	-.00734	-.00444	-.00471	-.00390	-5.17	-3.10	-15.3
5	716.0	-1.89	-1.82	----	-.00466	-.00474	-------	-.00884	-.00933	-------	-4.63	-2.80	-----
6	632.0	-1.58	-1.52	----	.00749	.00757	-------	-.0253	-.0268	-------	-2.12	-1.30	-----
7	615.0	-1.48	-1.42	----	.0113	.0114	-------	-.0301	-.0318	-------	-1.37	-.83	-----
8	571.0	-1.37	-1.32	-1.52	.0165	.0166	.0164	-.0347	-.0368	-.0305	-.52	-.35	-1.39
9	524.8	-1.16	-1.12	----	.0227	.0229	-------	-.0406	-.0430	-------	1.11	.68	-----
10	478.5	-.96	-.93	----	.0301	.0302	-------	-.0461	-.0487	-------	2.66	1.60	-----
11	432.2	-.77	-.74	----	.0397	.0399	-------	-.0484	-.0513	-------	3.97	2.38	-----
12	386.0	-.60	-.58	-.64	.0236	.0241	.0237	-.0265	-.0286	-.0196	6.08	3.65	2.00
13	353.0	-.52	-.50	----	.0401	.0404	-------	-.00802	-.0114	-------	5.90	3.53	-----
14	306.3	-.25	-.25	----	.0936	.0936	-------	.0552	.0587	-------	5.03	3.03	-----
15	259.6	.02	.07	----	.153	.152	-------	.123	.128	-------	4.18	2.53	-----
16	212.9	.28	.27	----	.212	.212	-------	.167	.178	-------	3.35	2.08	-----
17	166.2	.58	.56	----	.238	.238	-------	.170	.194	-------	2.27	1.45	-----
18	119.5	.93	.84	1.00	.238	.237	.237	.259	.275	.168	.99	.73	1.00
19	85.3	.92	.88	.97	.281	.281	-------	.332	.347	-------	1.07	1.00	-----
20	0	.92	.89	----	.288	.288	.282	.377	.395	.396	1.00	1.00	1.00
29	663.6	-1.94	-1.86	----	-.00594	.00603	-------	-.0190	-.0201	-------	-4.99	-3.00	-----
30	652.1	-1.93	-1.85	----	-.00570	.00578	-------	-.0145	-.0153	-------	-4.90	-2.95	-----
37	30.9	1.00	1.00	1.00	1.00	1.00	1.00	1.00	1.00	1.00	1.41	8.45	-----
38	52.9	1.07	1.07	1.09	1.77	1.77	1.71	-.954	-.958	-.874	1.70	10.23	-----

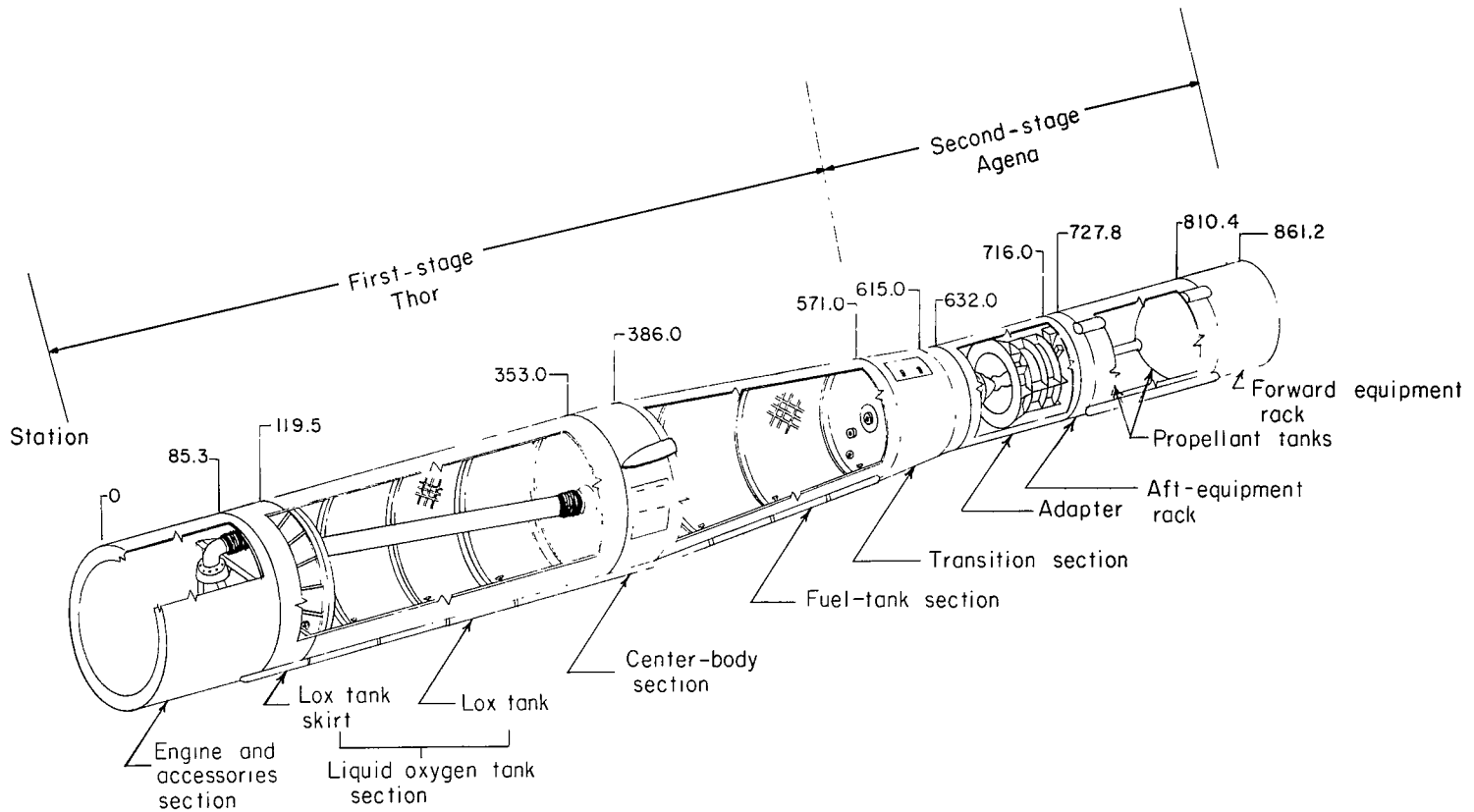

Figure 1.- Schematic cutaway of test vehicle.

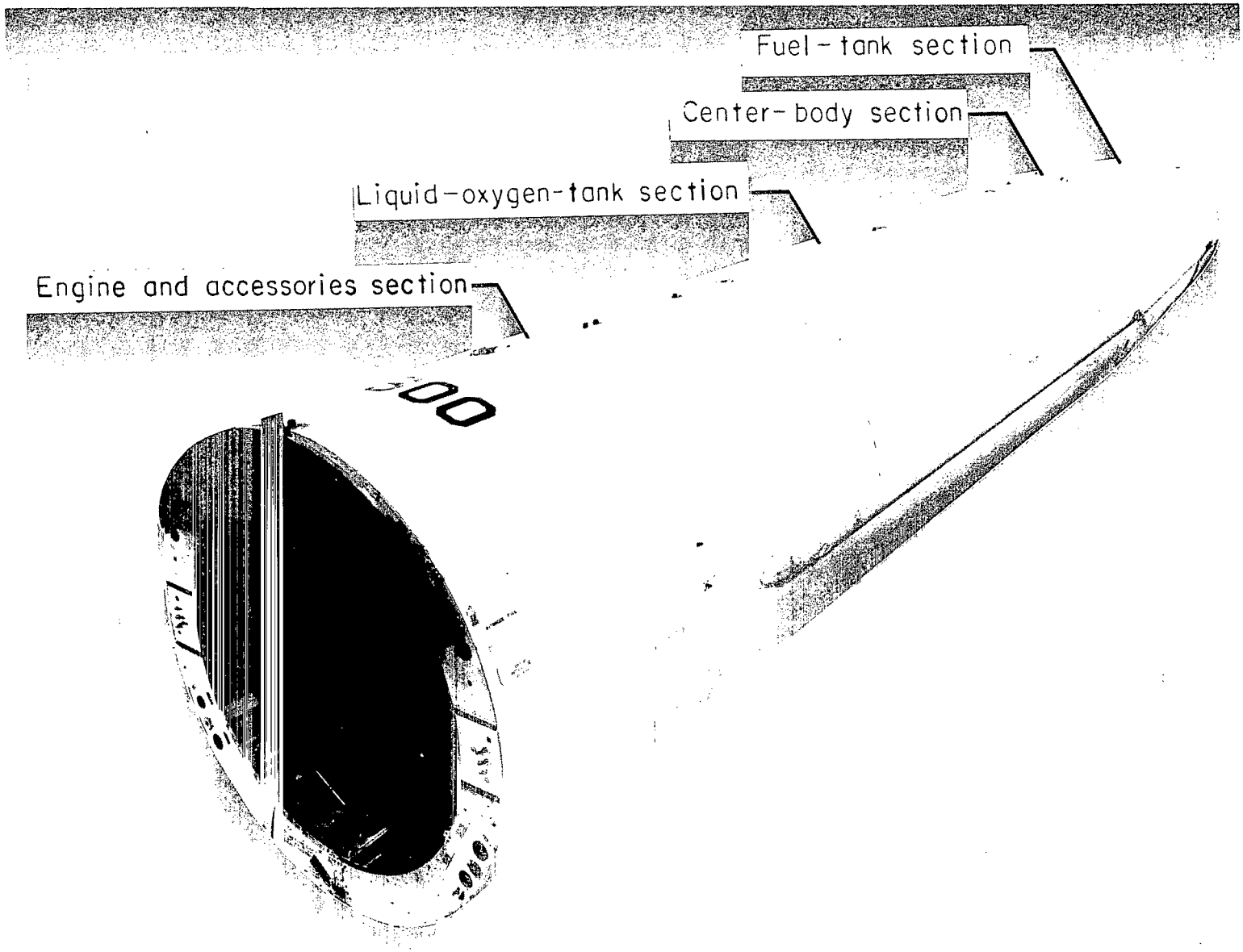

Figure 2.- First stage of test vehicle.

L-65-1727.1

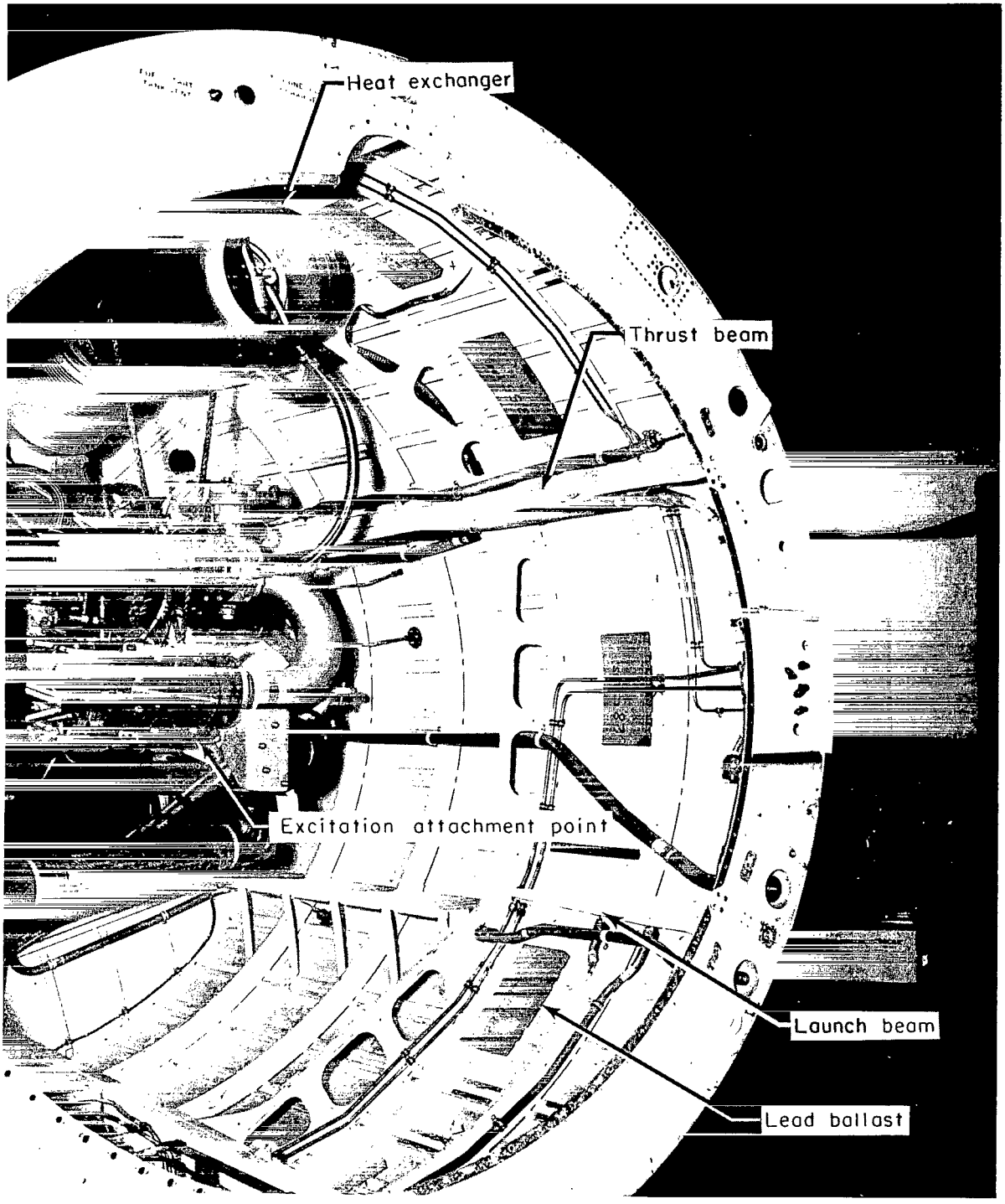

Figure 3.- Engine and accessories section. L-65-1610.1

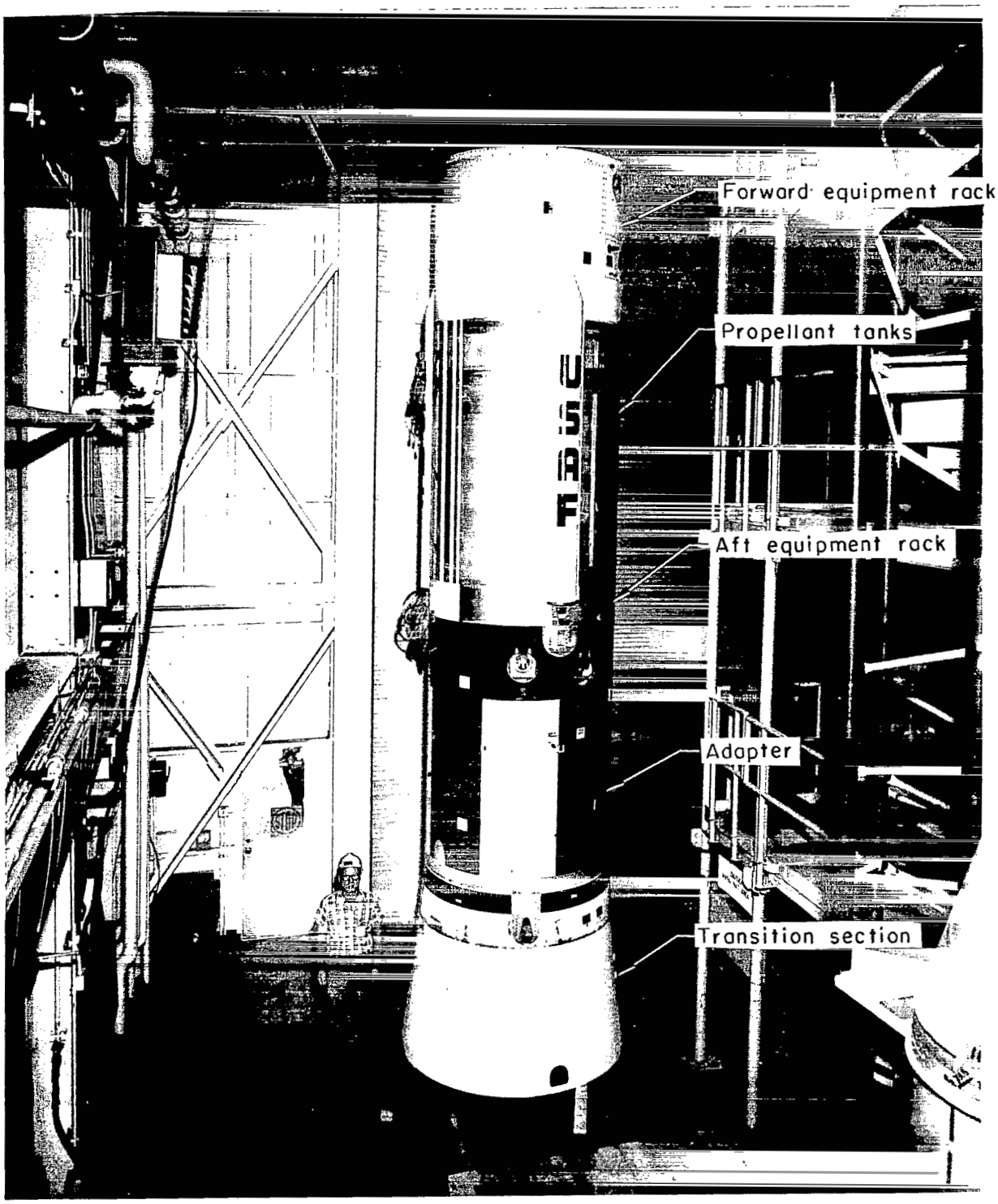

Figure 4.- Second stage of test vehicle. L-65-6254

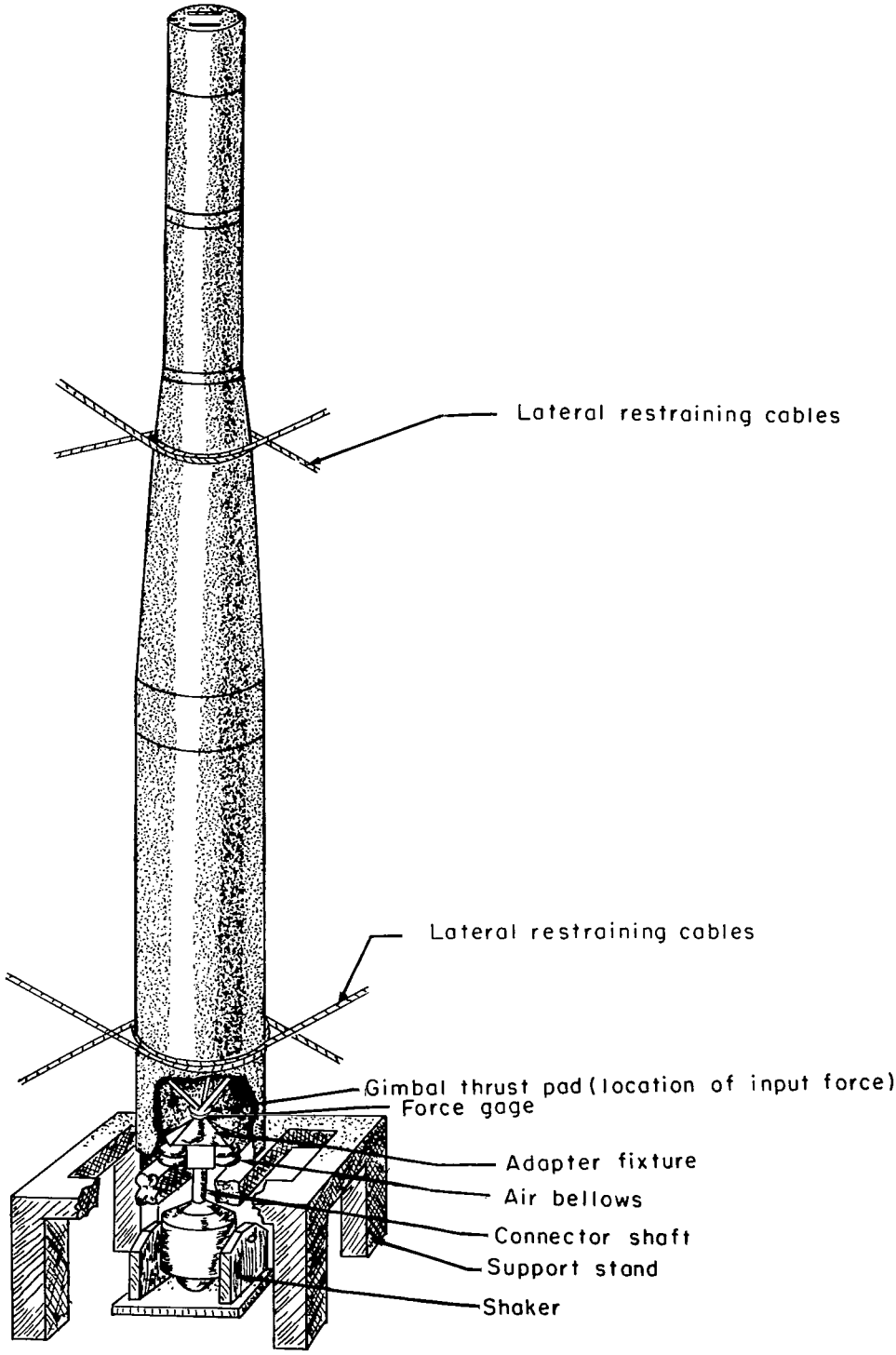

Figure 5.- Longitudinal support system for test vehicle.

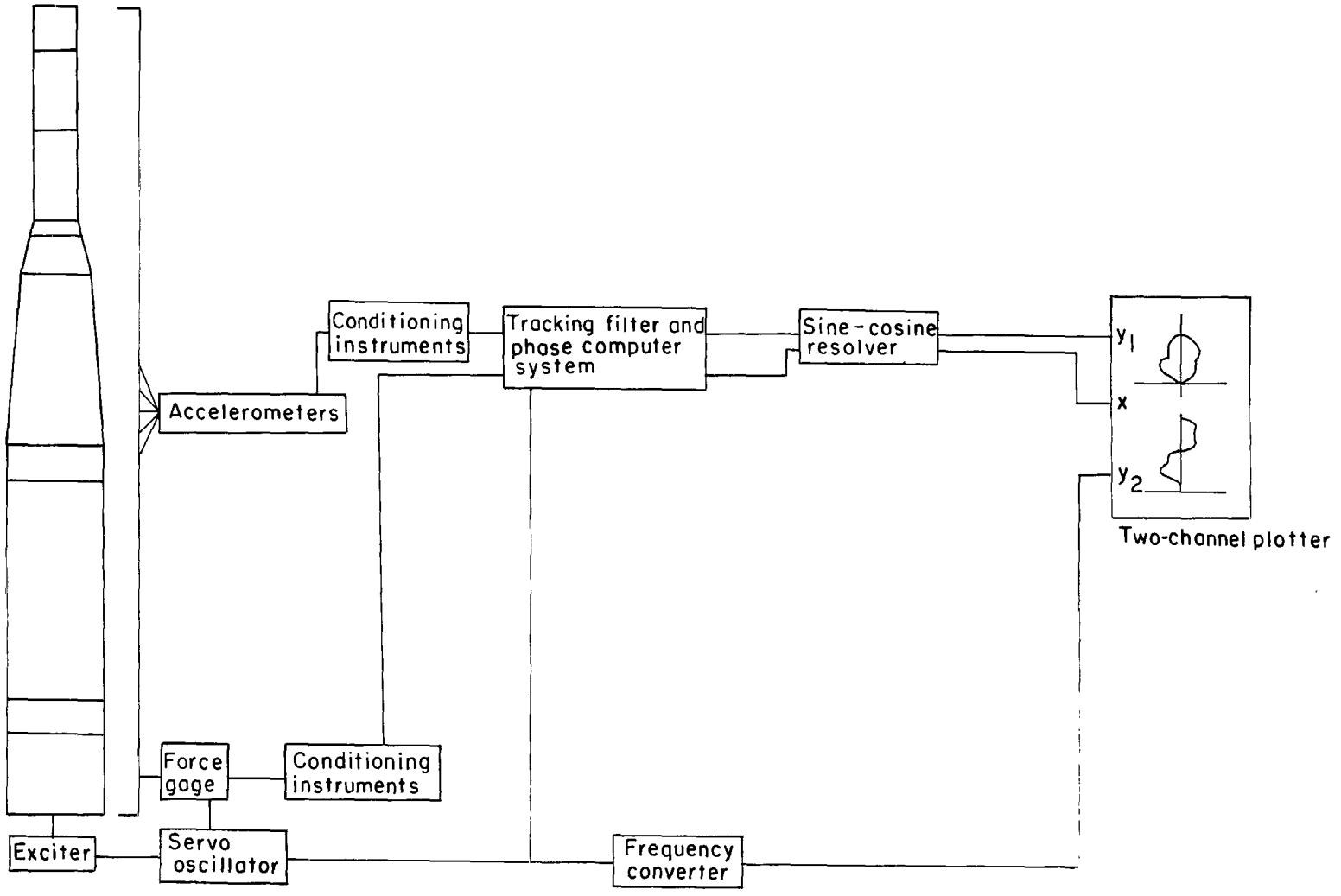

Figure 6.- Schematic of instrumentation used to obtain vector-response plots.

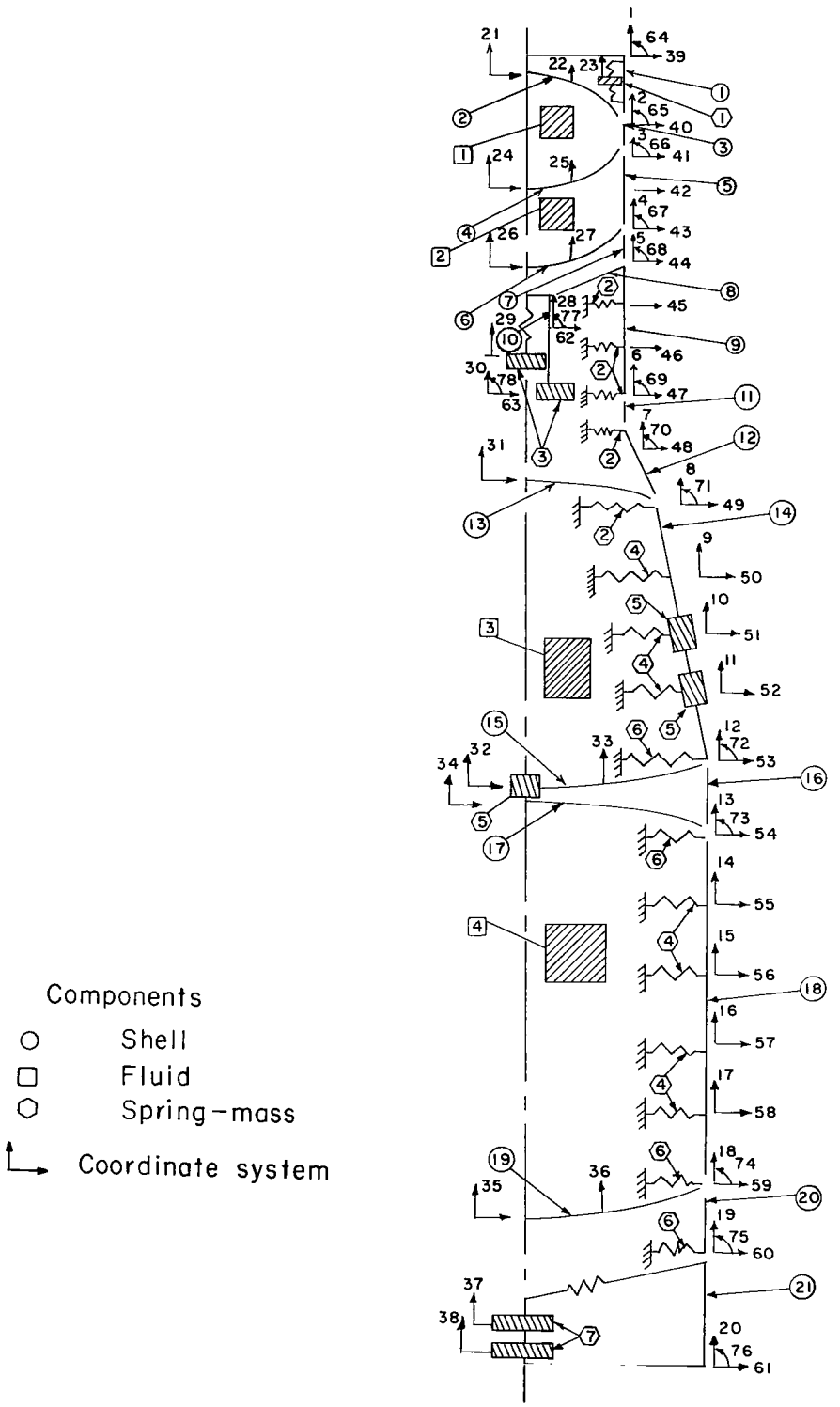

Figure 7.- Analytical model of the two-stage vehicle and coordinate system.

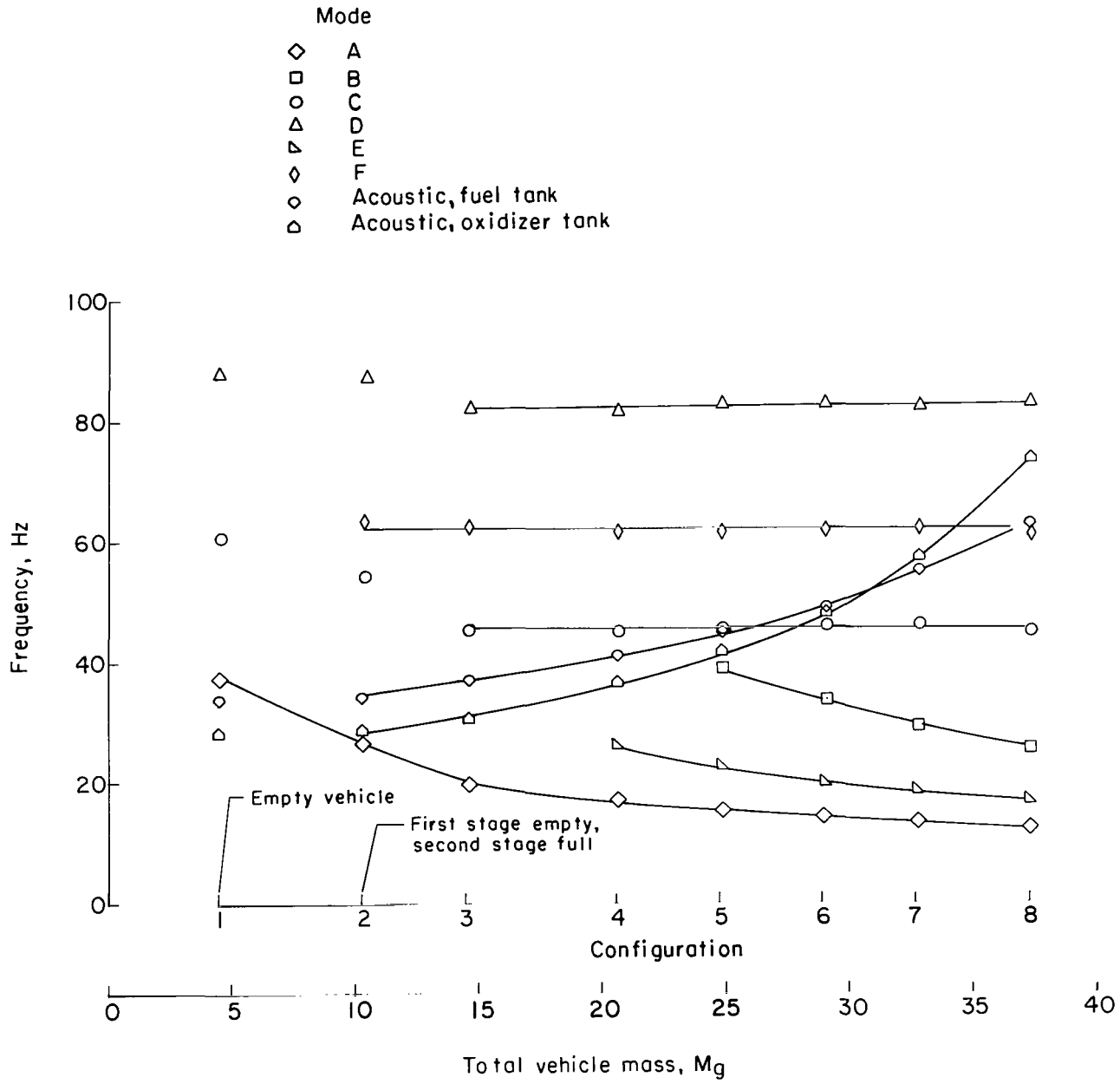

Figure 8.- Variation of resonant frequencies of associated modes.

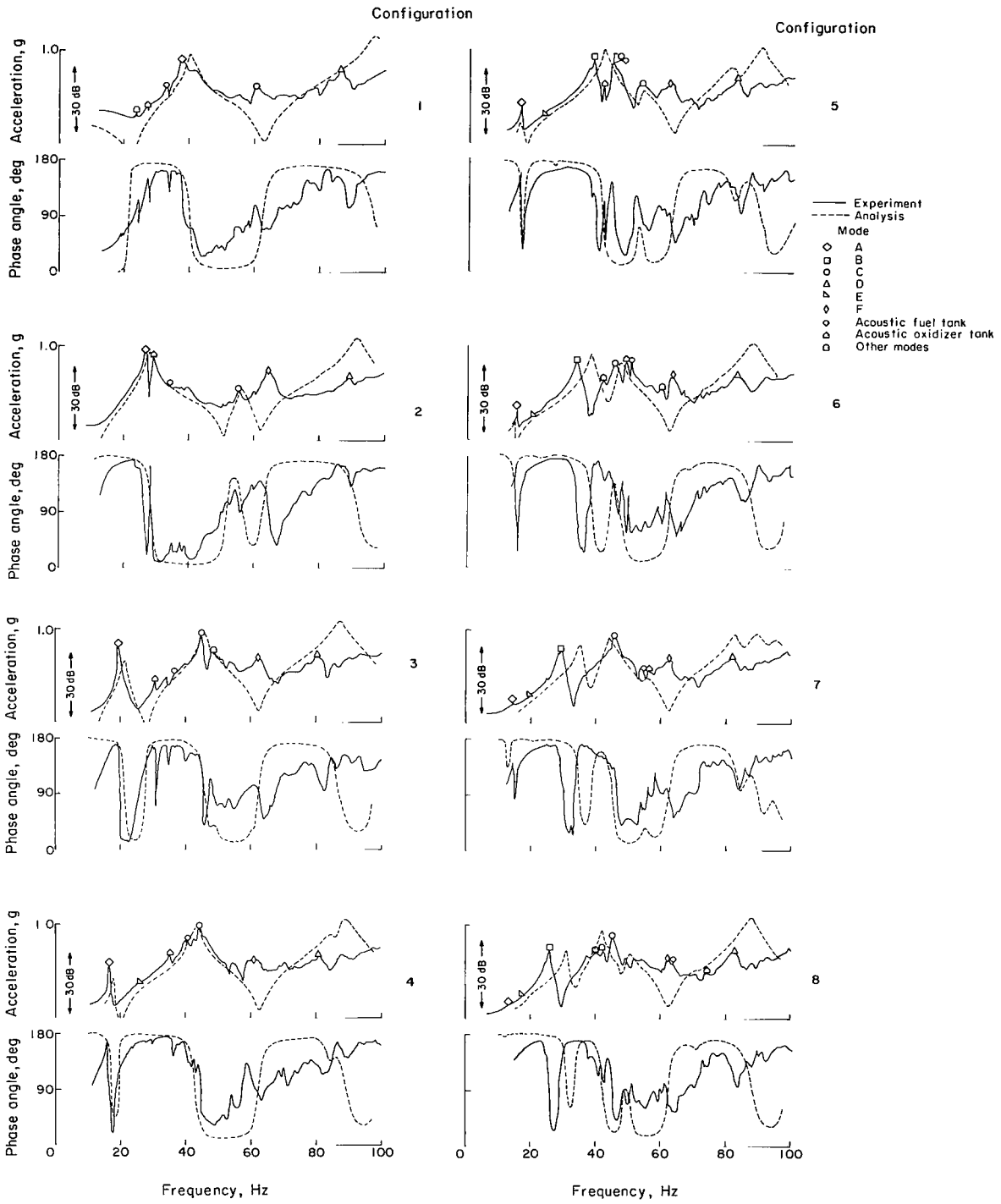

Figure 9.- Frequency response of the thrust structure at station 30.9 for various vehicle configurations.

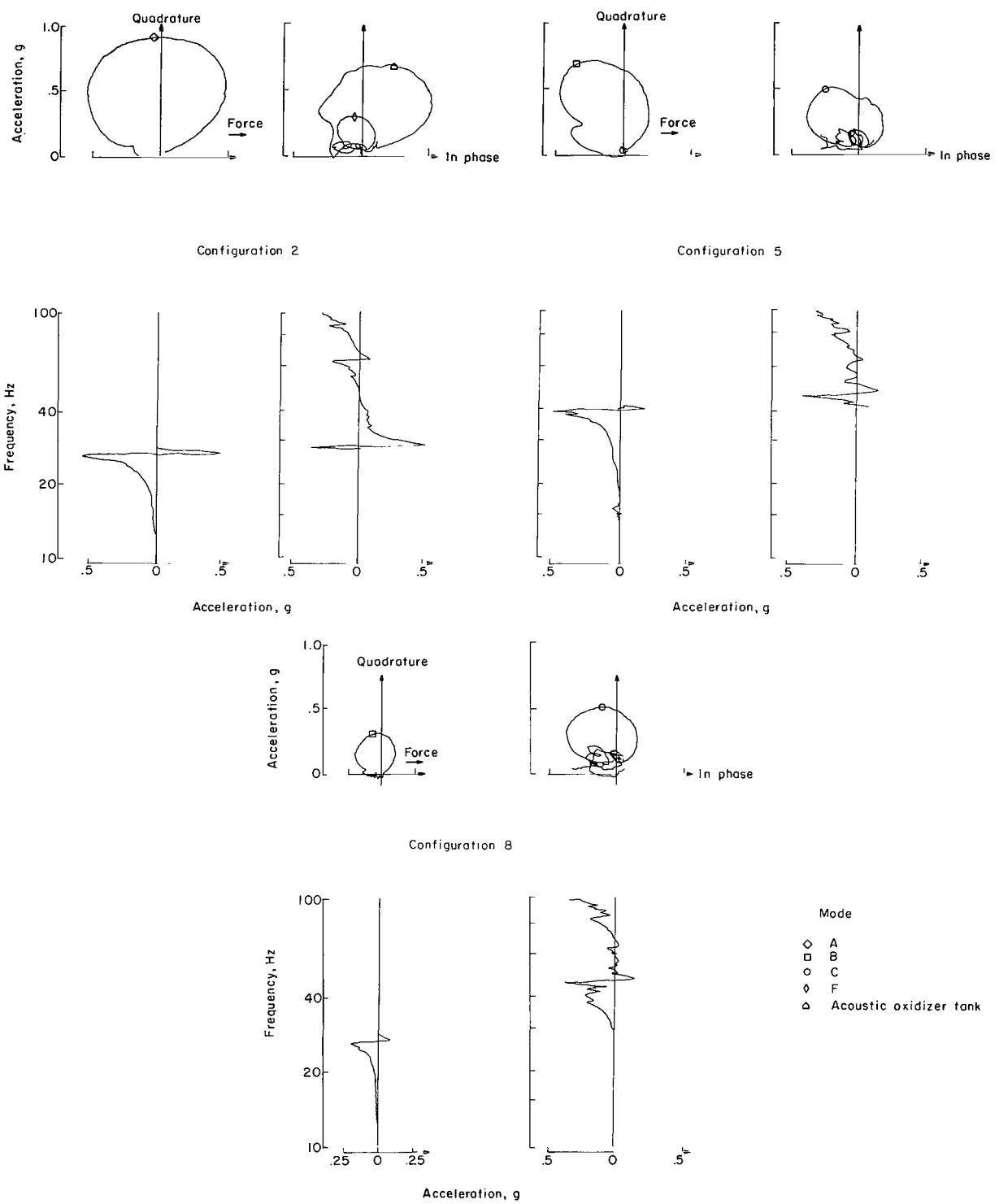

Figure 10.- Typical vector-response plots of thrust structure acceleration.

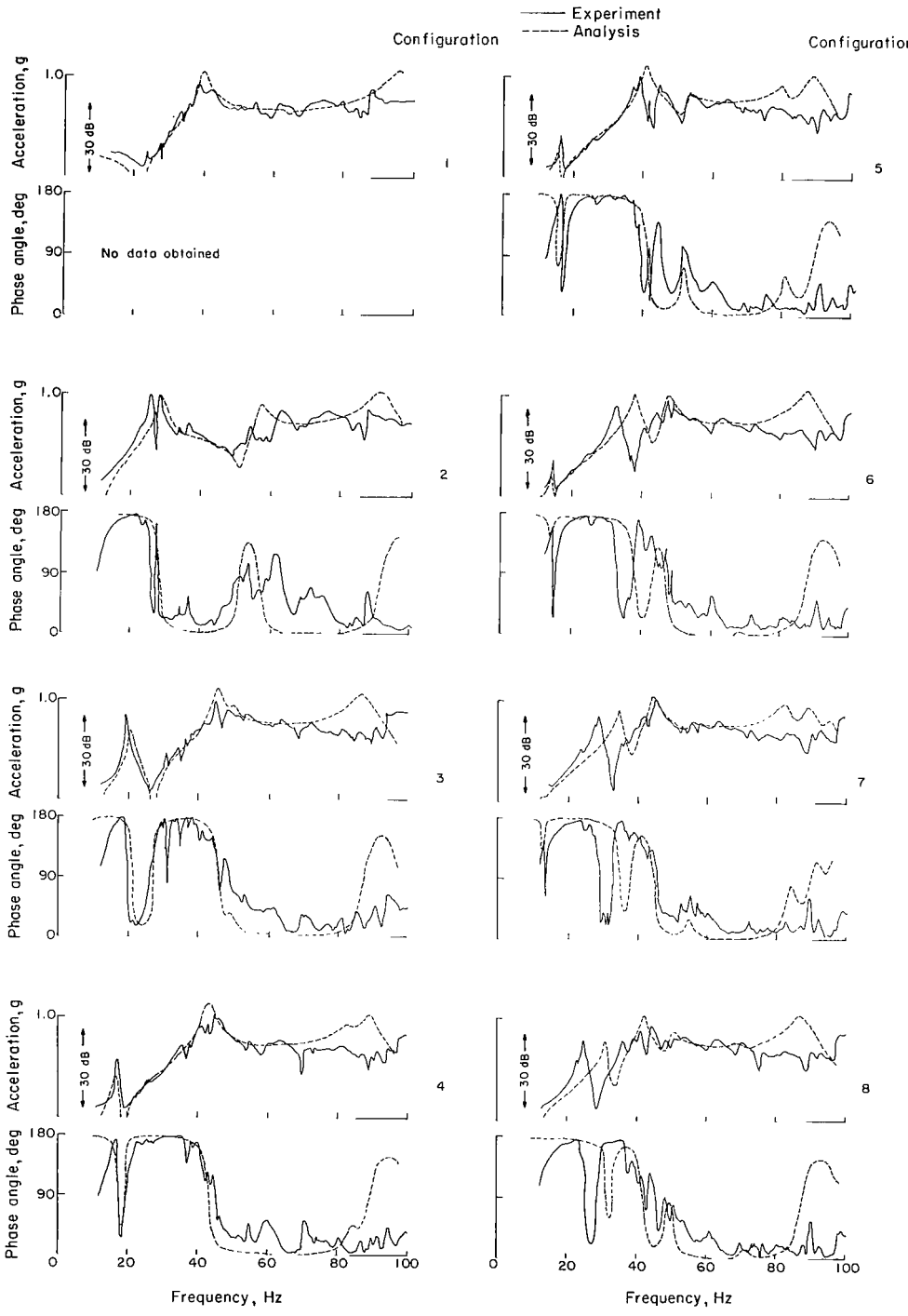

Figure 11.- Frequency response of the turbopump for various vehicle configurations.

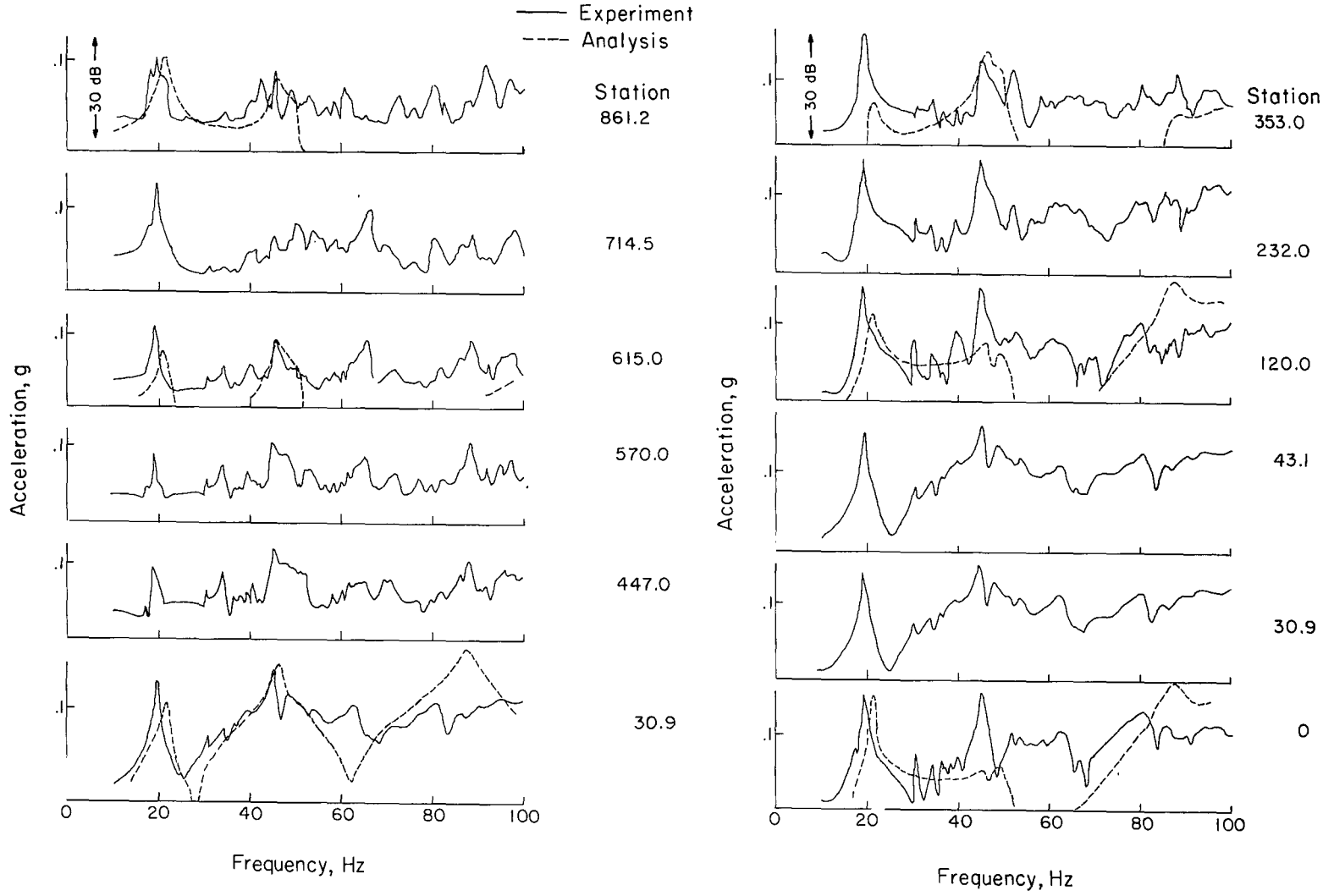

Figure 12.- Variation of accelerations measured along the length of the vehicle for configuration 3.

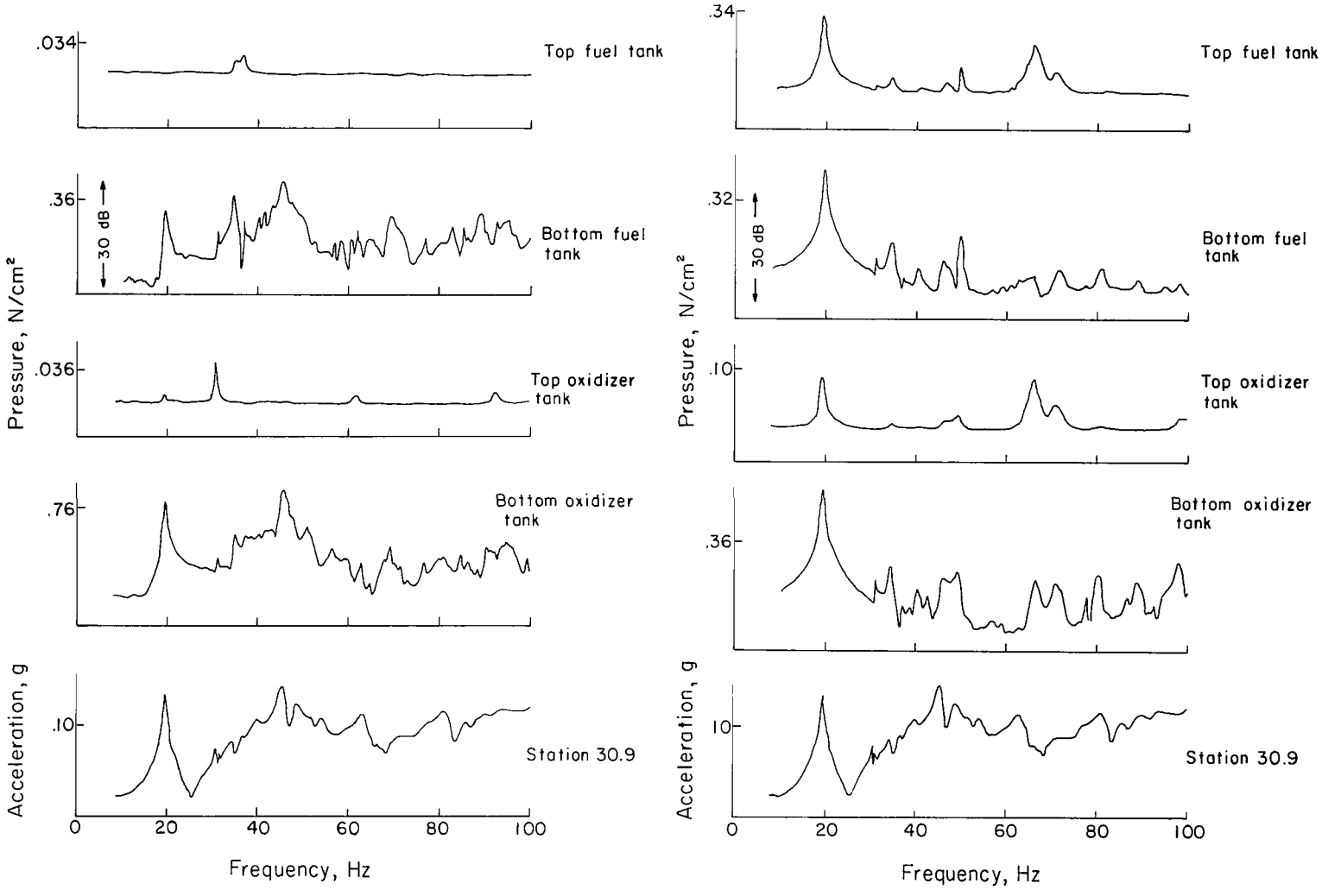

Figure 13.- Pressure variations at top and bottom of propellant tanks for configuration 3.

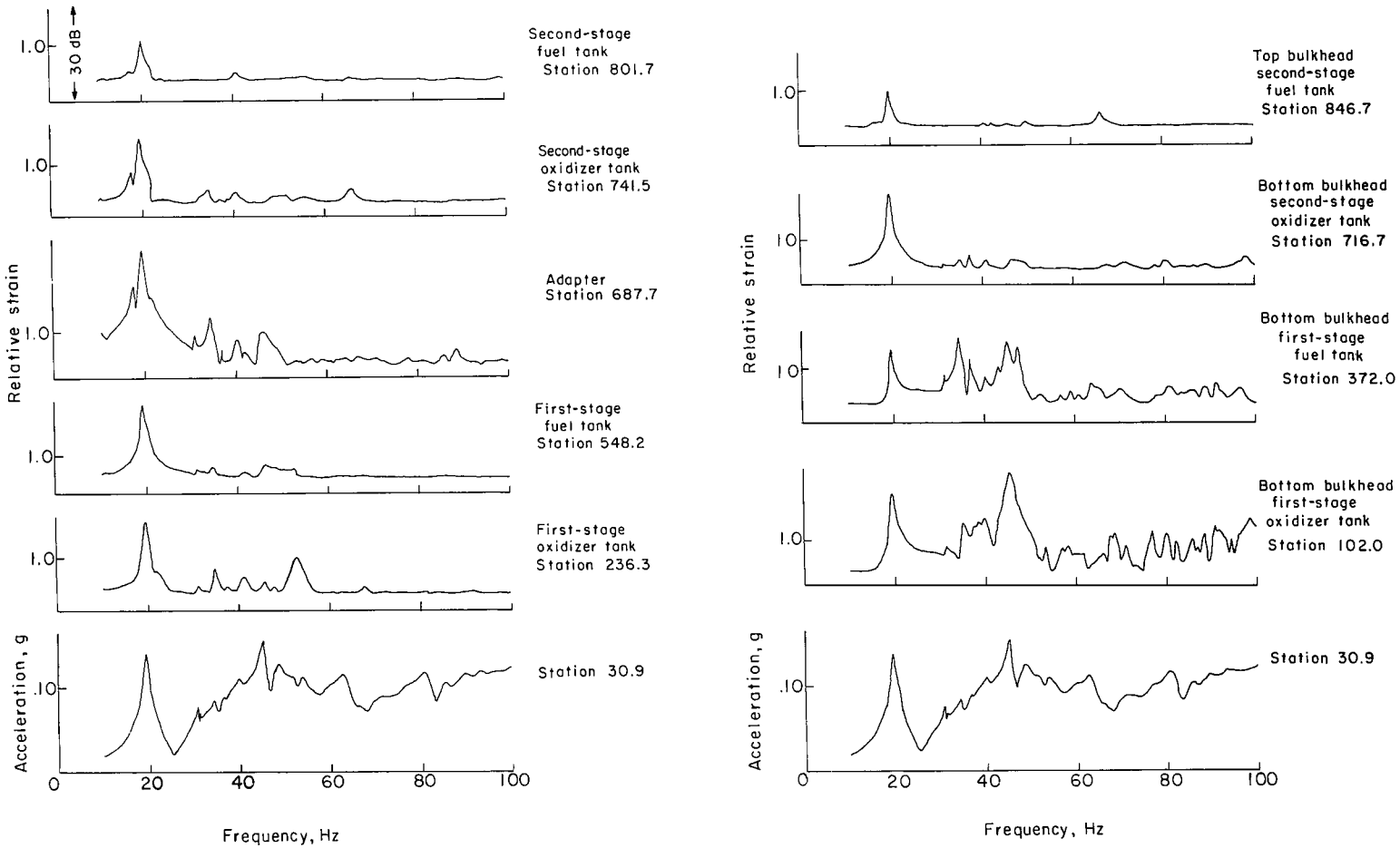

Figure 14.- Strain variations measured for configuration 3.

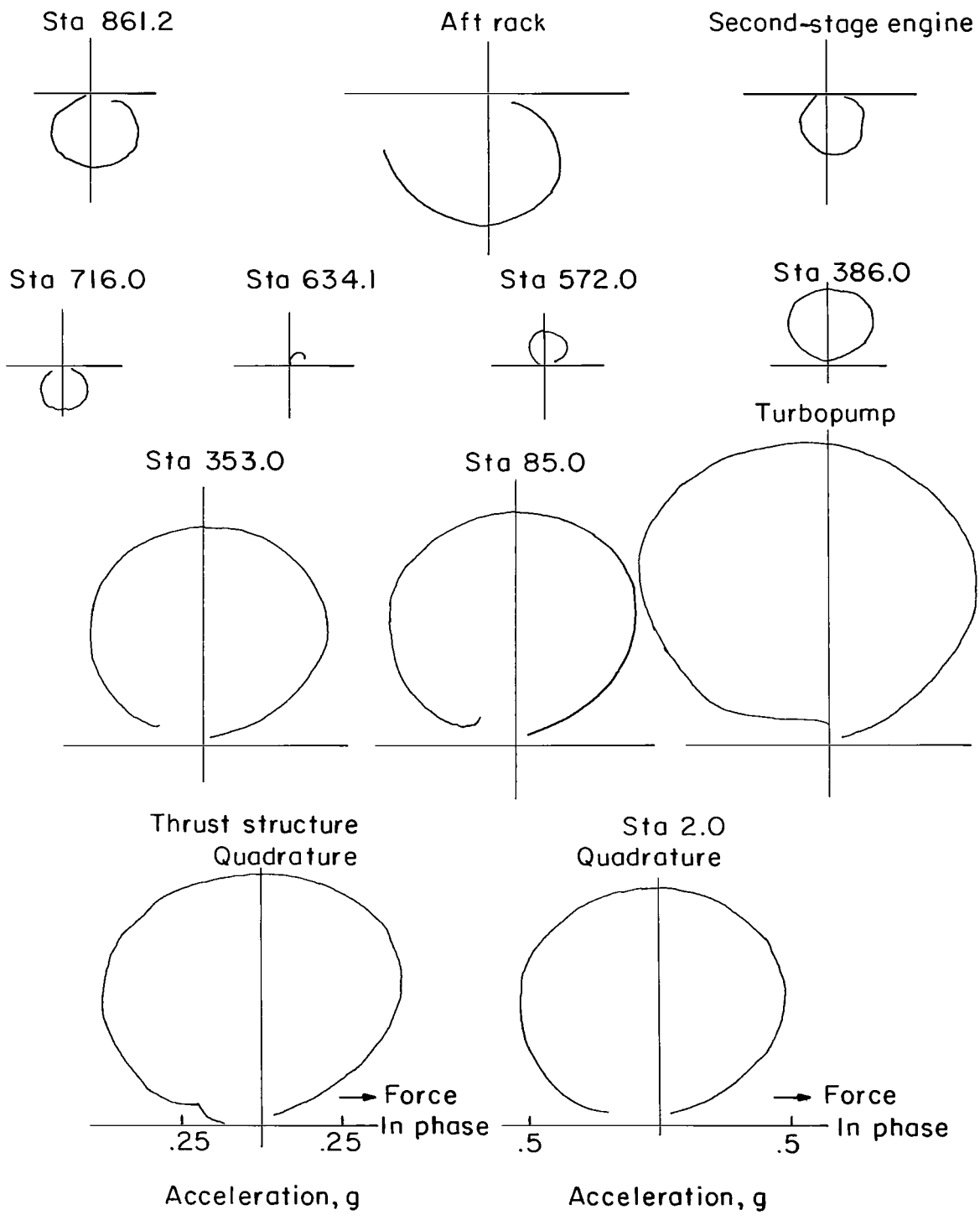

Figure 15.- Vector-response plots of acceleration measured along the vehicle length for mode A of configuration 2.

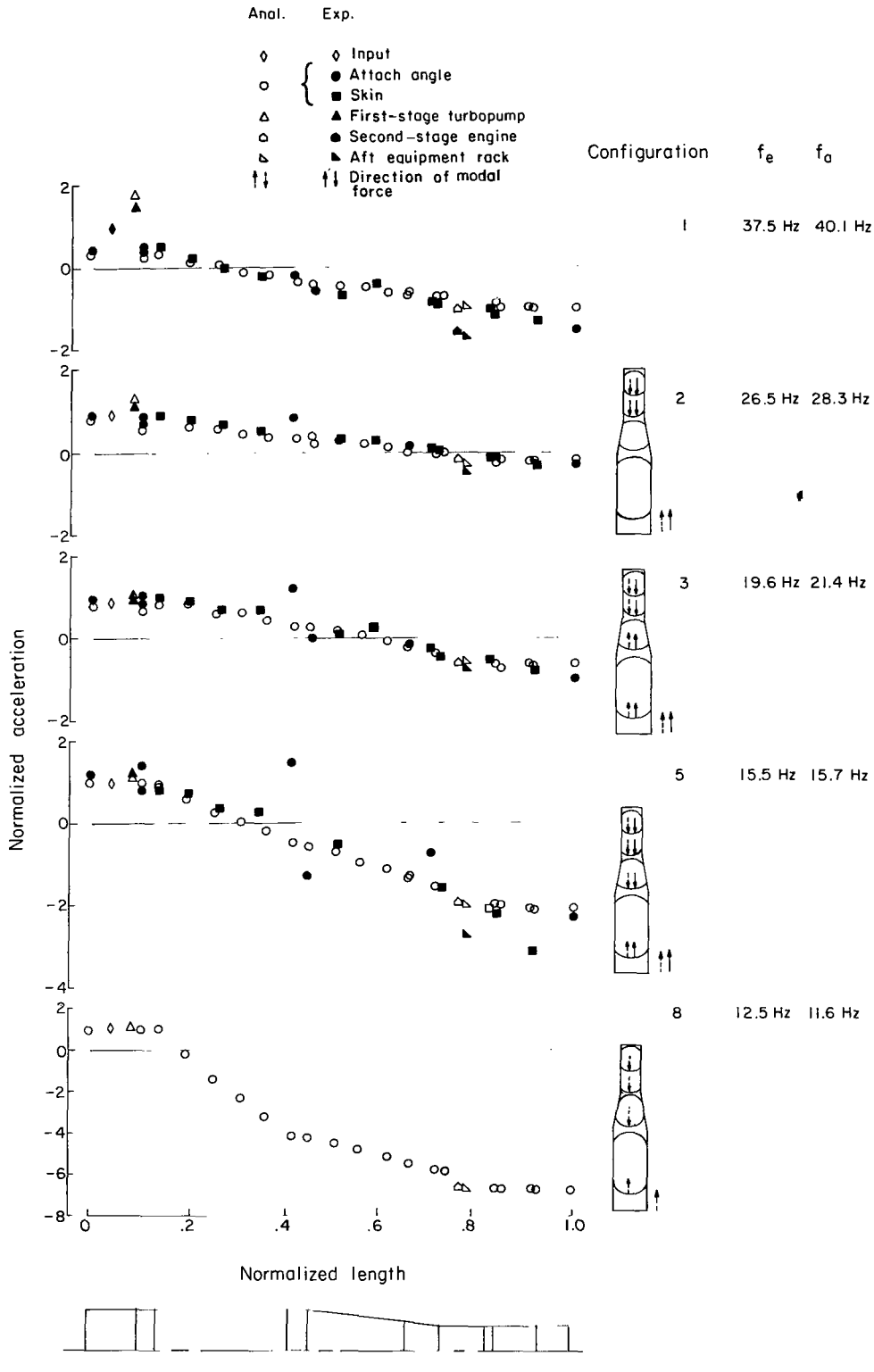

Figure 16.- Resonant response shapes and predicted mode shapes of mode A.

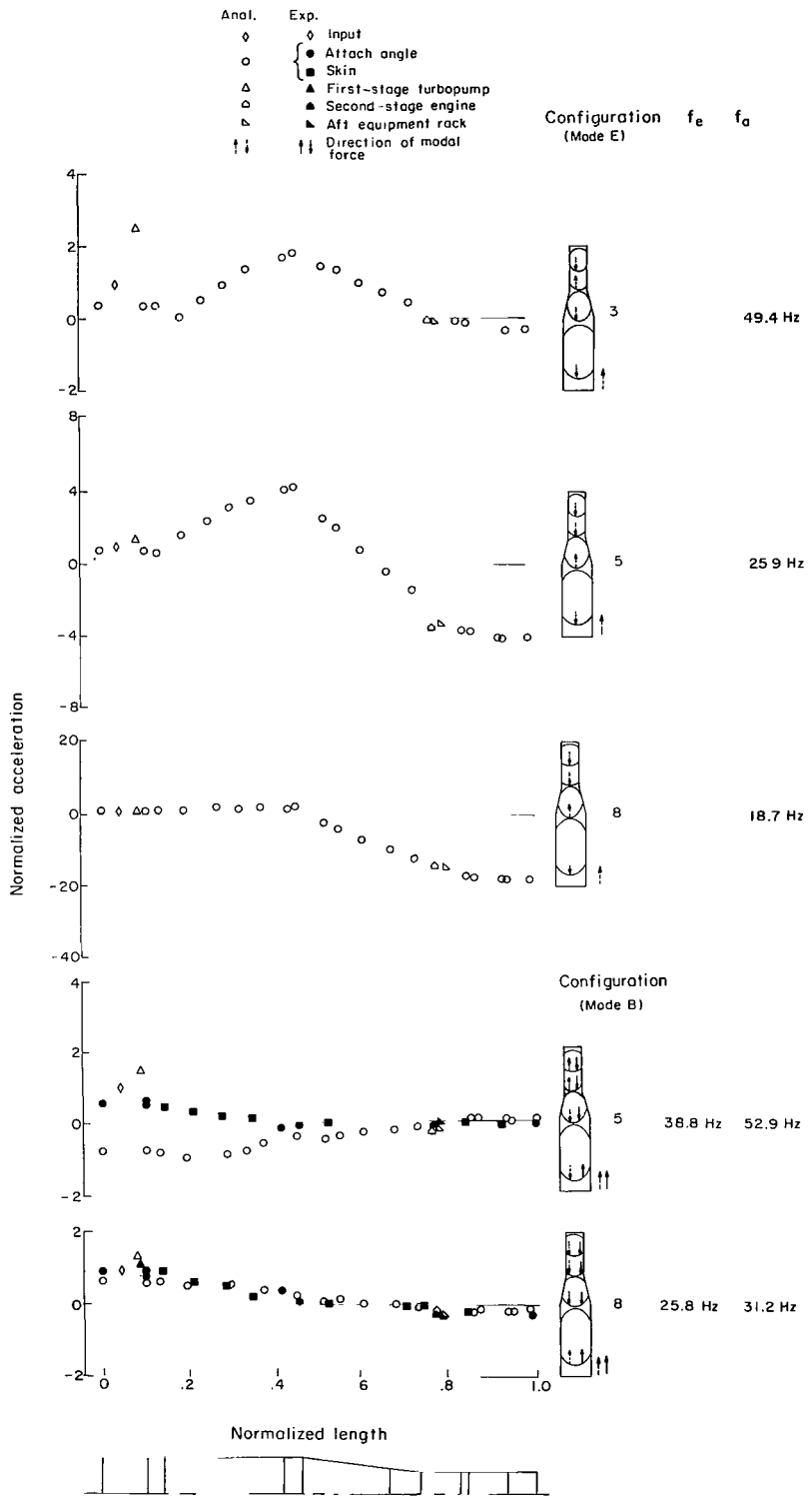

Figure 17.- Resonant response shapes and predicted mode shapes of modes B and E.

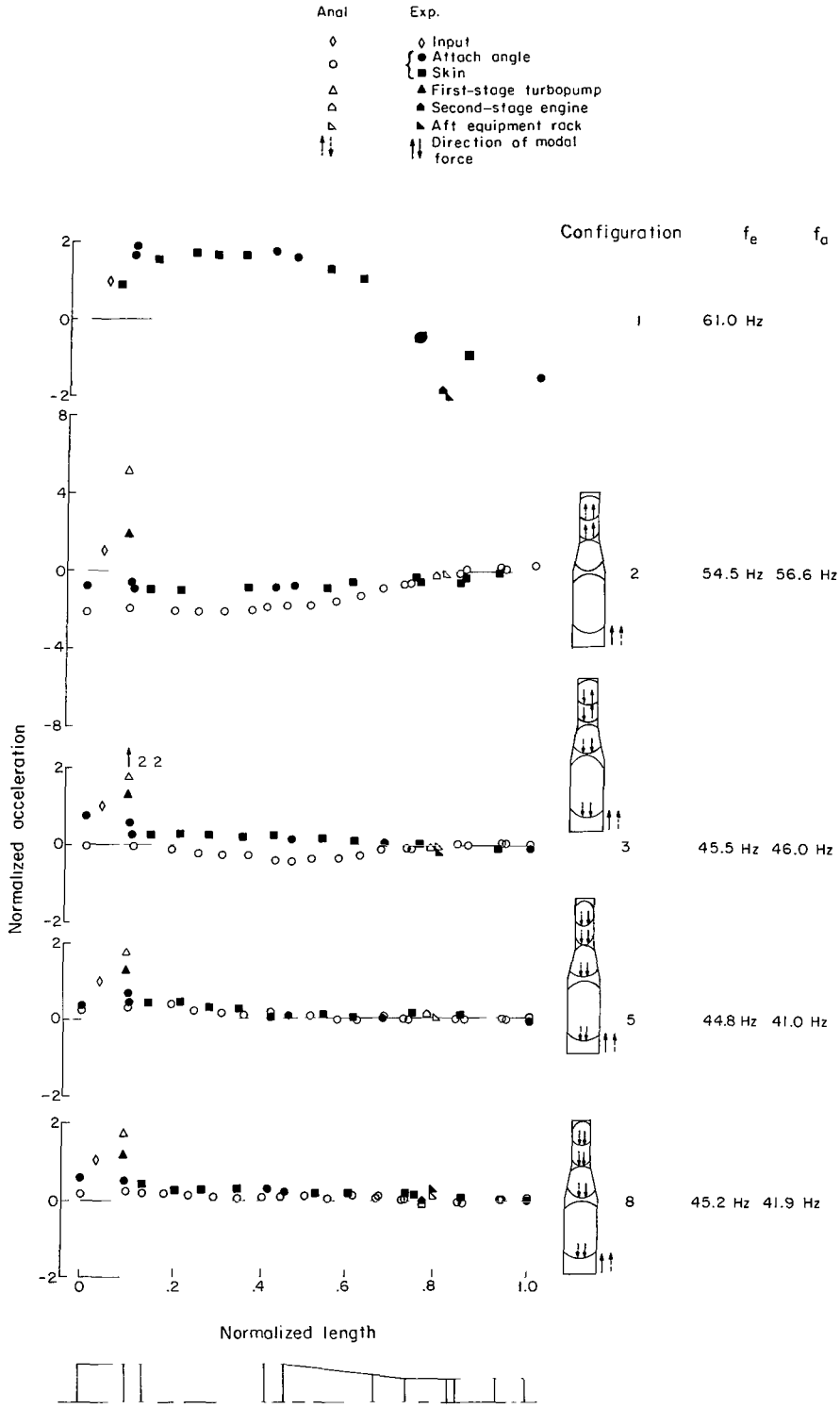

Figure 18.- Resonant response shapes and predicted mode shapes of mode C.

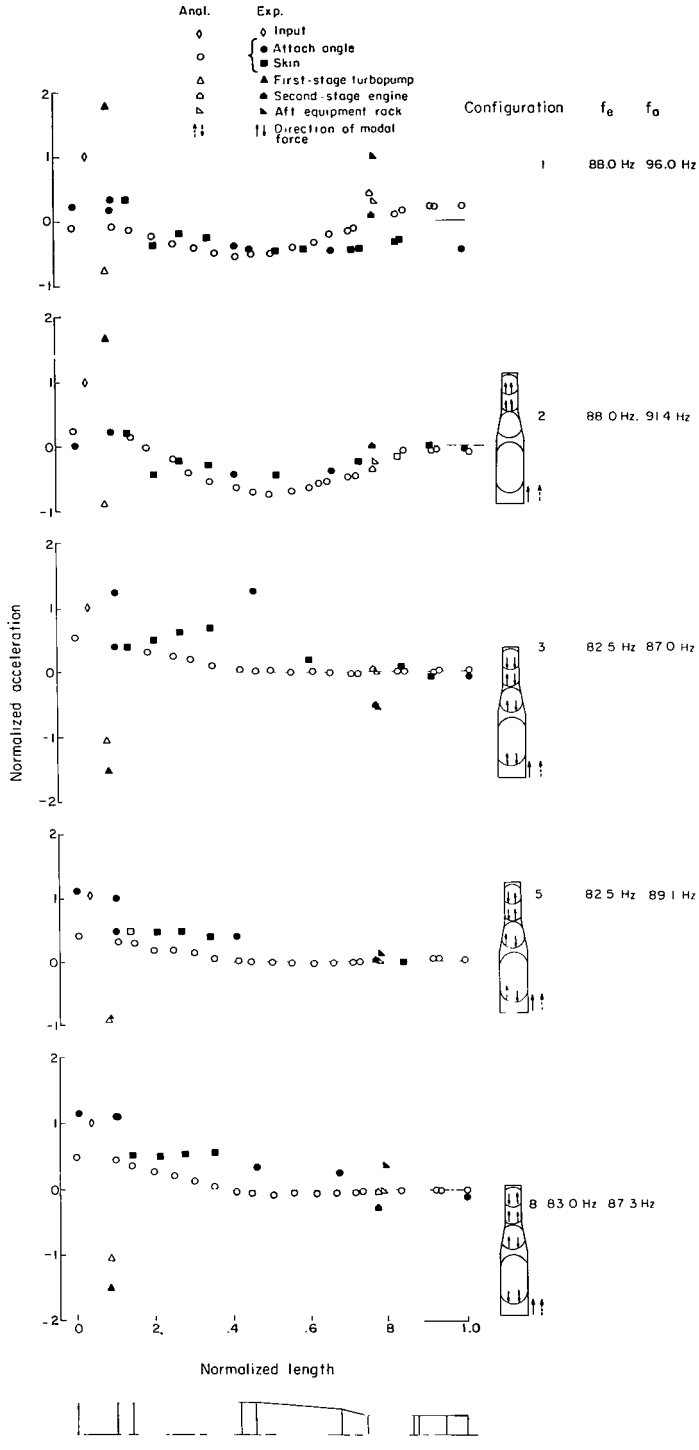

Figure 19.- Resonant response shapes and predicted mode shapes of mode D.

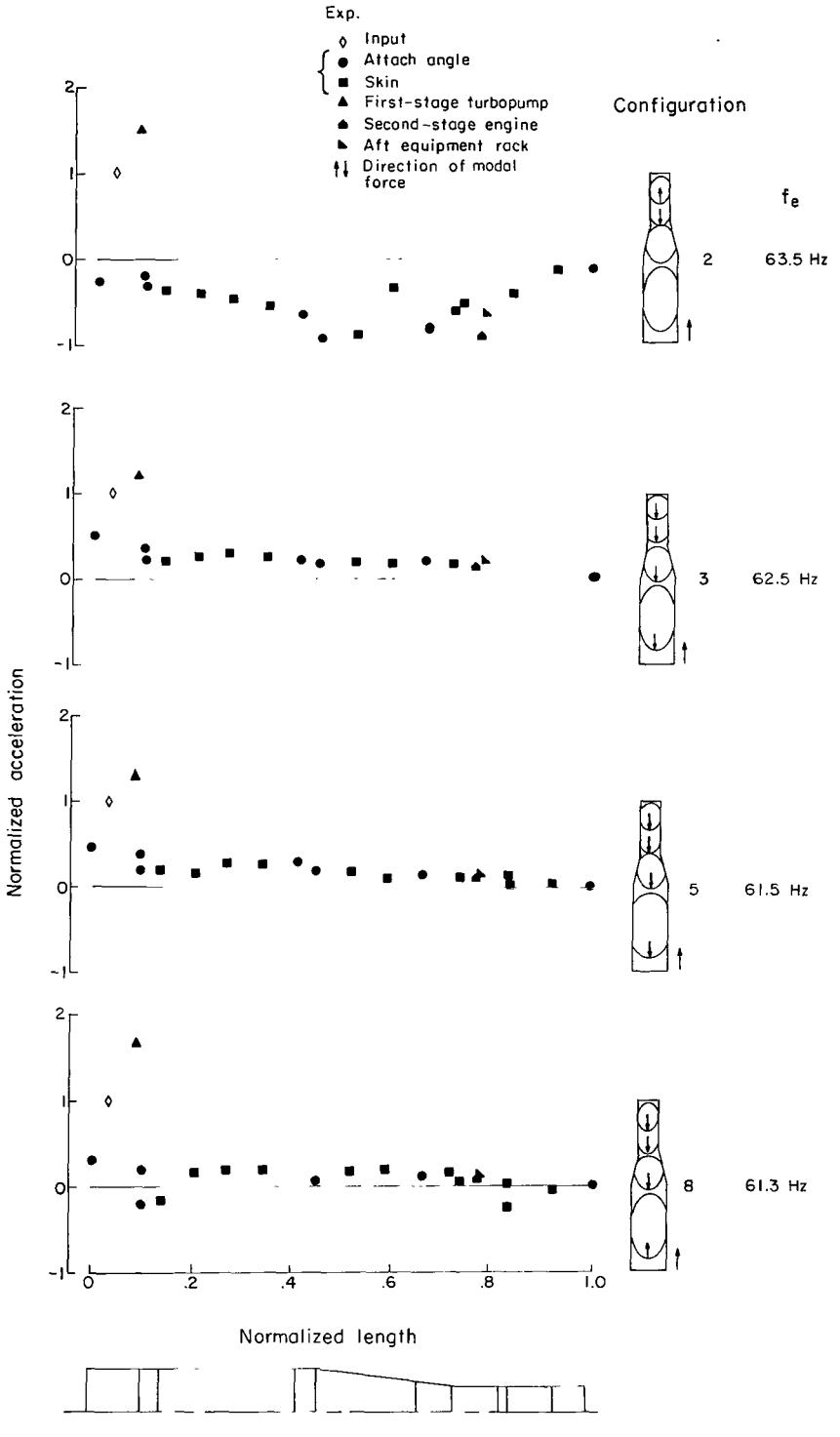

Figure 20.- Resonant response shapes of mode F.

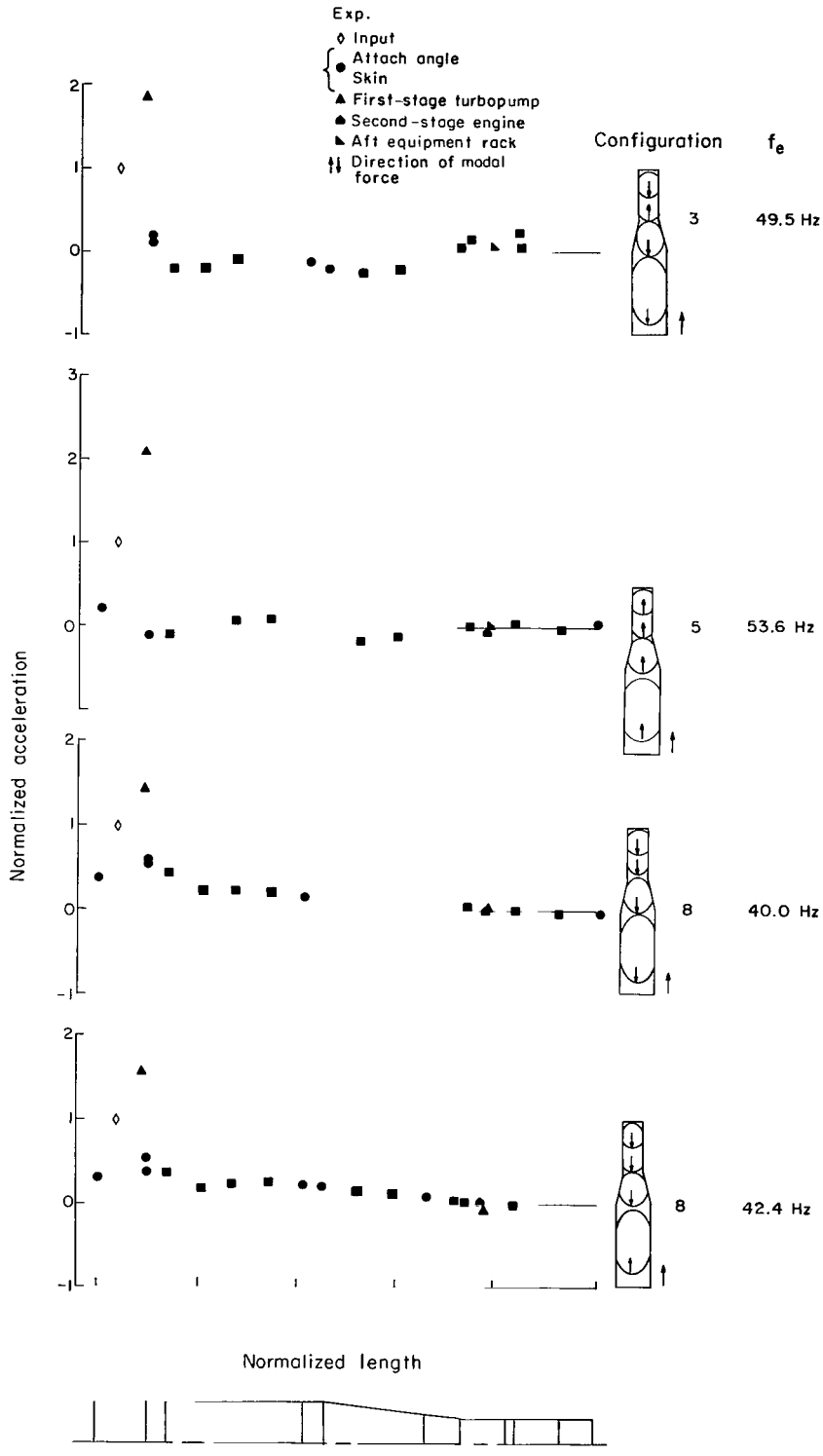

Figure 21.- Resonant response shapes of other modes.

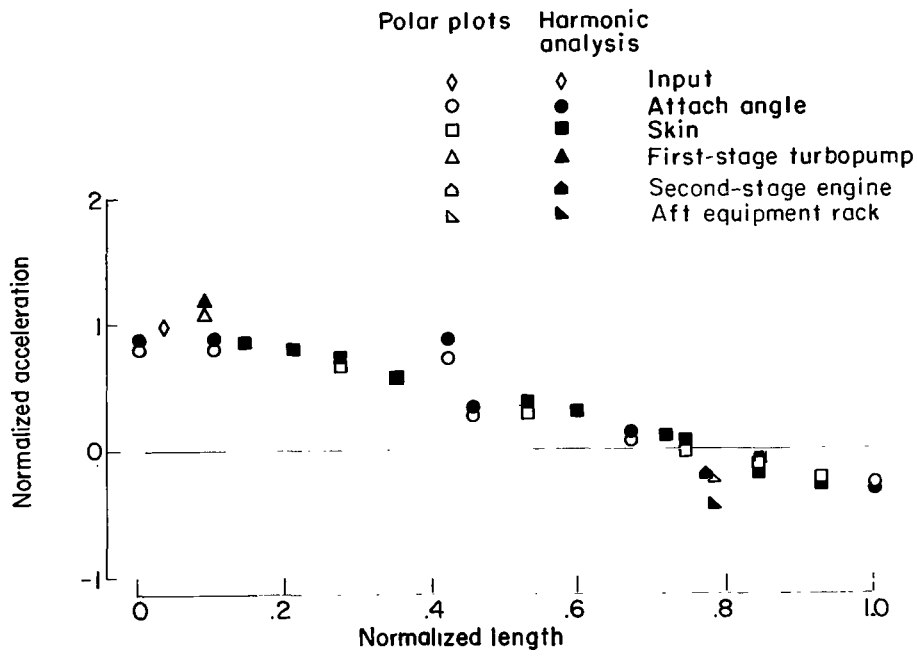

(a) Configuration 2; mode A. Resonant frequencies 26.4 Hz and 26.5 Hz for vector response and harmonic analysis, respectively.

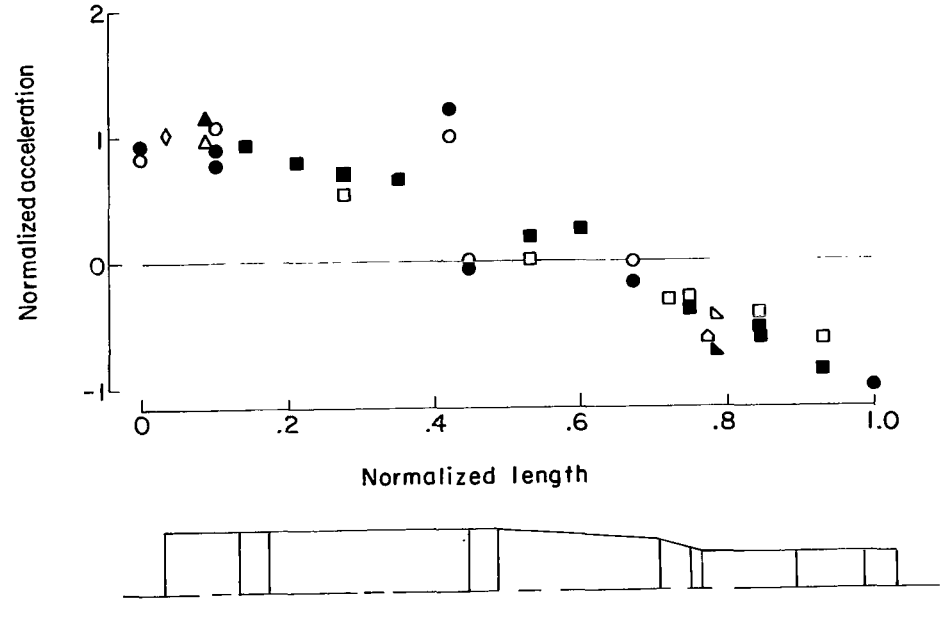

(b) Configuration 3; mode A. Resonant frequencies 19.7 Hz and 19.6 Hz for vector response and harmonic analysis, respectively.

Figure 22.- Comparison of response shapes obtained from vector-response plots and harmonic analysis of experimental data.

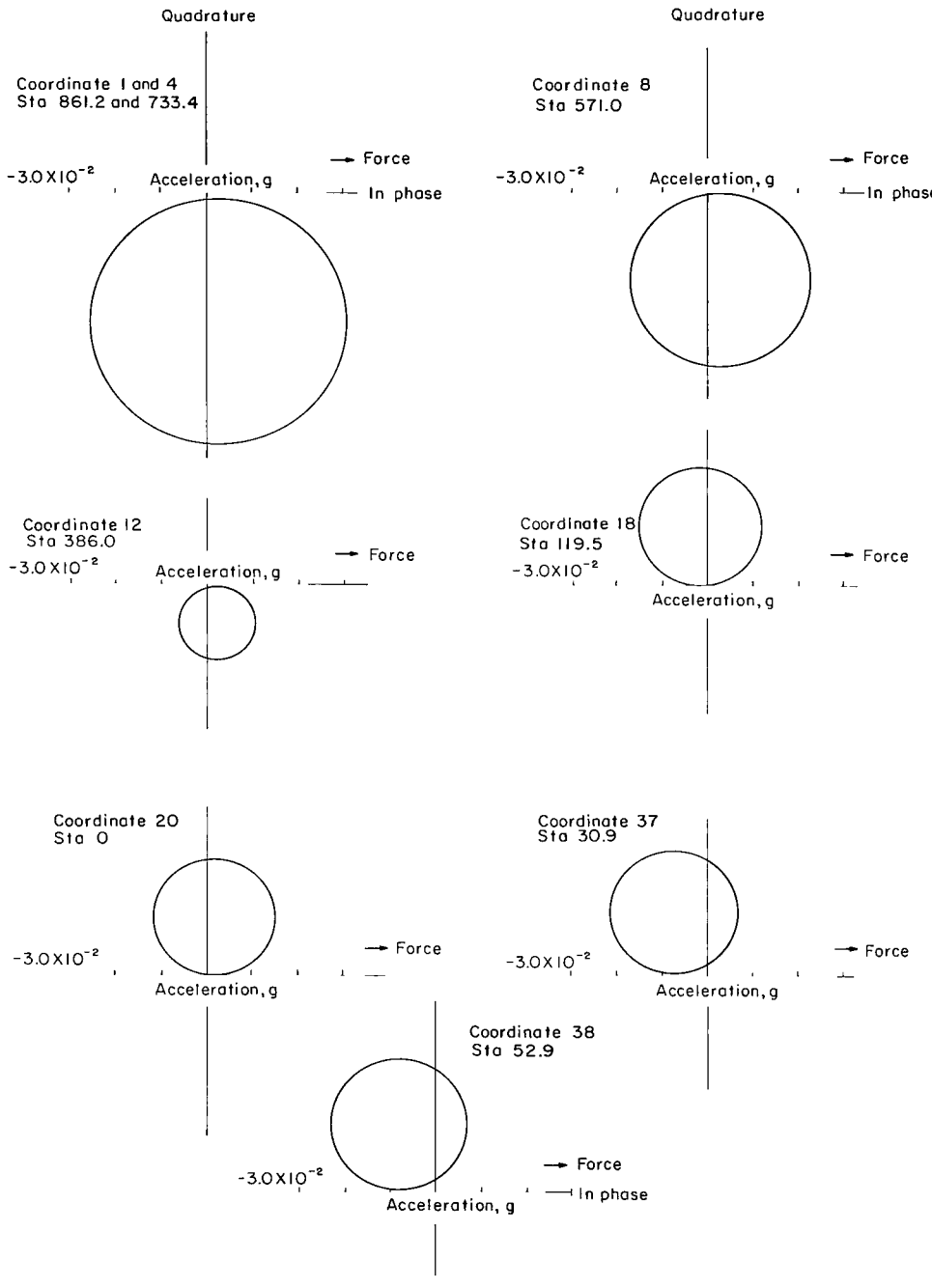

(a) Mode A.

Figure 23.- Vector-response plots of best circles drawn through the acceleration vector predicted by forced response analysis for configuration 5.

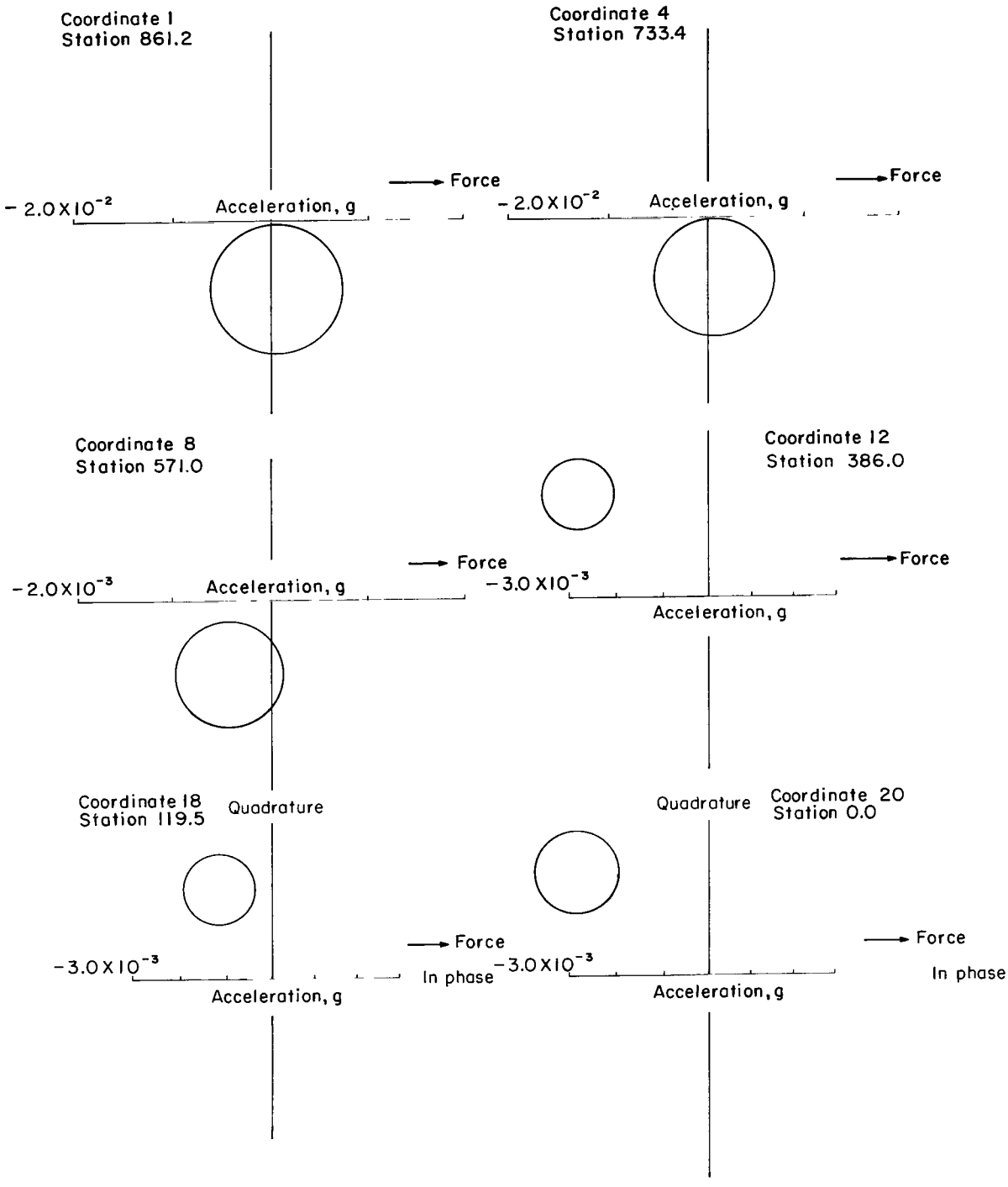

(b) Mode E.

Figure 23.- Concluded.

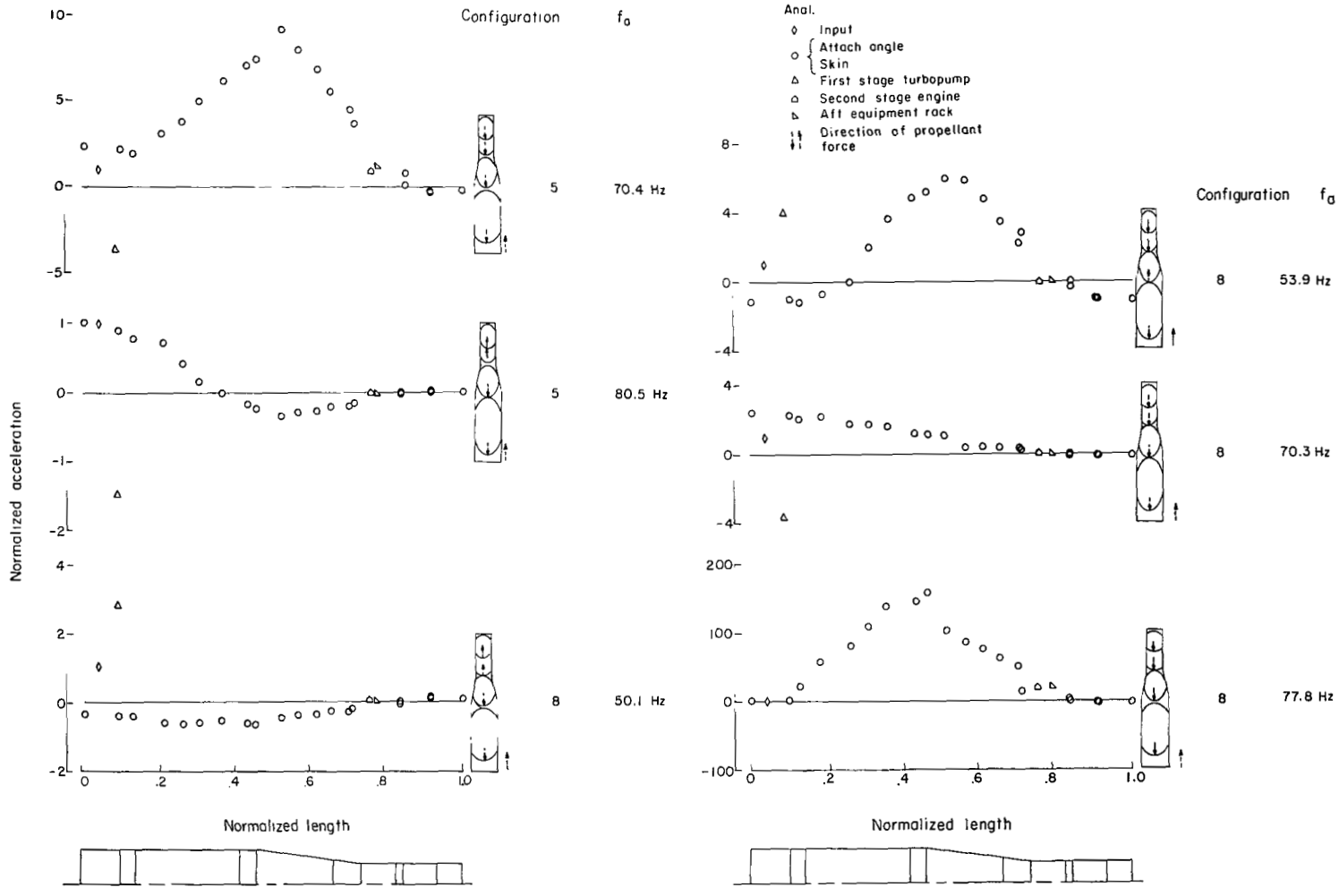

Figure 24.- Predicted mode shapes of other modes.

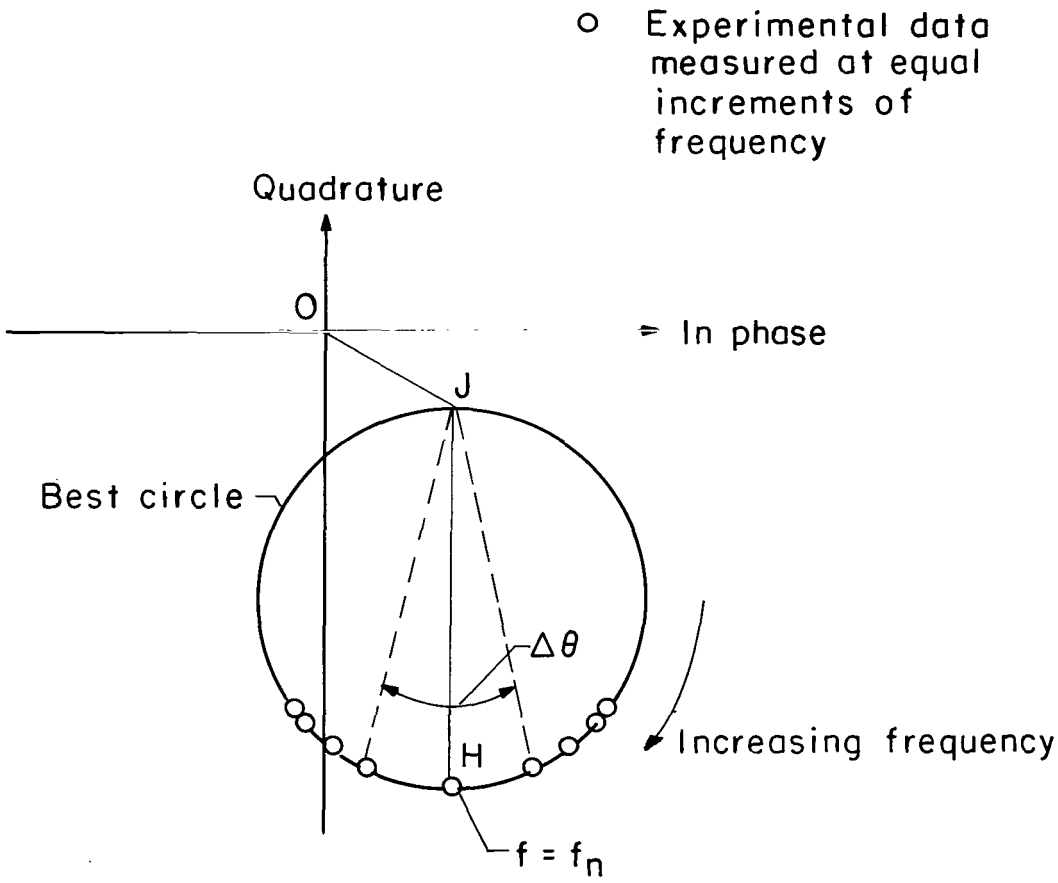

Figure 25.- Vector-response plot at a resonance of a typical system having more than one degree of freedom. (Taken from ref. 15.)

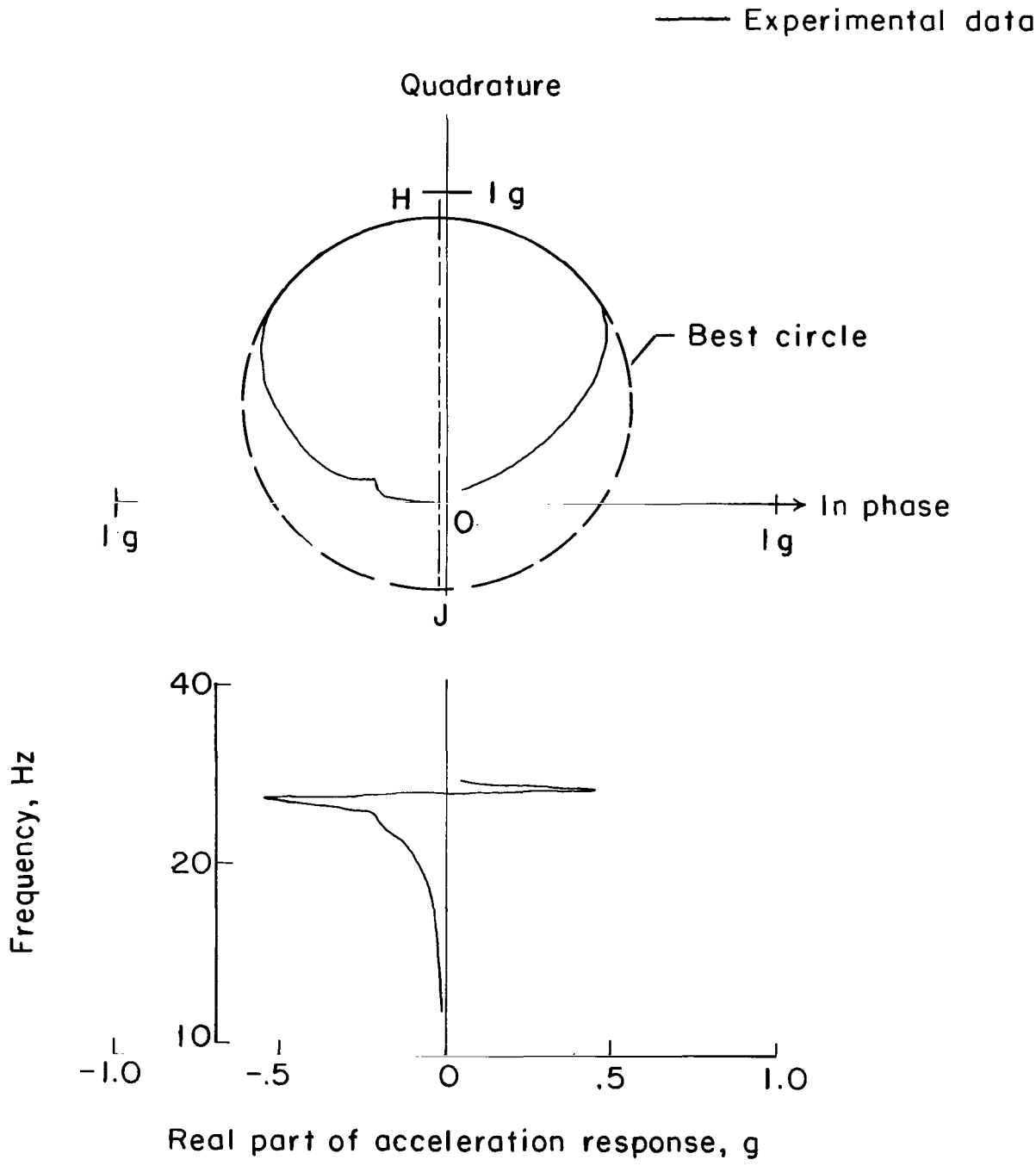

Figure 26.- Typical plot of acceleration vector recorded during frequency sweep tests. Mode A, configuration 2.

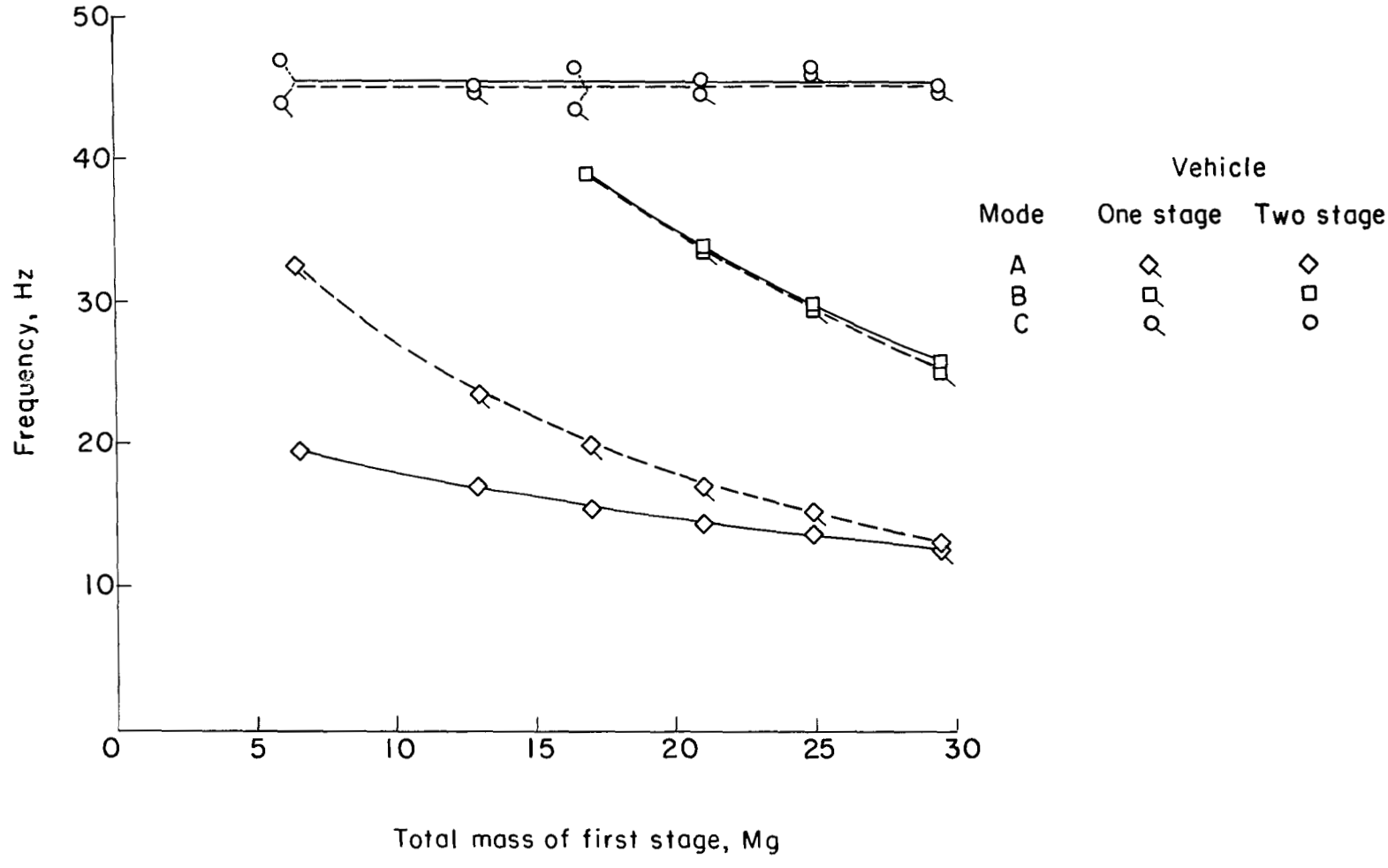

Figure 27.- Comparison of related modes obtained for one-stage and two-stage vehicles.

NATIONAL AERONAUTICS AND SPACE ADMINISTRATION
WASHINGTON, D. C. 20546
OFFICIAL BUSINESS

FIRST CLASS MAIL

POSTAGE AND FEES PAID
NATIONAL AERONAUTICS AND
SPACE ADMINISTRATION

"The aeronautical and space activities of the United States shall be conducted so as to contribute . . . to the expansion of human knowledge of phenomena in the atmosphere and space. The Administration shall provide for the widest practicable and appropriate dissemination of information concerning its activities and the results thereof."

—NATIONAL AERONAUTICS AND SPACE ACT OF 1958

NASA SCIENTIFIC AND TECHNICAL PUBLICATIONS

TECHNICAL REPORTS: Scientific and technical information considered important, complete, and a lasting contribution to existing knowledge.

TECHNICAL NOTES: Information less broad in scope but nevertheless of importance as a contribution to existing knowledge.

TECHNICAL MEMORANDUMS: Information receiving limited distribution because of preliminary data, security classification, or other reasons.

CONTRACTOR REPORTS: Scientific and technical information generated under a NASA contract or grant and considered an important contribution to existing knowledge.

TECHNICAL TRANSLATIONS: Information published in a foreign language considered to merit NASA distribution in English.

SPECIAL PUBLICATIONS: Information derived from or of value to NASA activities. Publications include conference proceedings, monographs, data compilations, handbooks, sourcebooks, and special bibliographies.

TECHNOLOGY UTILIZATION PUBLICATIONS: Information on technology used by NASA that may be of particular interest in commercial and other non-aerospace applications. Publications include Tech Briefs, Technology Utilization Reports and Notes, and Technology Surveys.

Details on the availability of these publications may be obtained from:

SCIENTIFIC AND TECHNICAL INFORMATION DIVISION

NATIONAL AERONAUTICS AND SPACE ADMINISTRATION

Washington, D.C. 20546